



Bifunctional $\text{H}_2\text{WO}_4/\text{TS-1}$ catalysts for direct conversion of cyclohexane to adipic acid: Active sites and reaction steps

Jing Dai, Wenzhou Zhong*, Wenjun Yi, Mengqiao Liu, Liquiu Mao*, Qiong Xu, Dulin Yin

National & Local United Engineering Laboratory for New Petrochemical Materials & Fine Utilization of Resources, Key Laboratory of Chemical Biology
Traditional Chinese Medicine Research Ministry of Education, College of Chemistry and Chemical Engineering, Hunan Normal University, Changsha 410081,
PR China

ARTICLE INFO

Article history:

Received 25 January 2016

Received in revised form 28 March 2016

Accepted 5 April 2016

Available online 7 April 2016

Keywords:

Cyclohexane

Adipic acid

Bifunctional catalyst

$\text{H}_2\text{WO}_4/\text{TS-1}$

Hydrogen peroxide

ABSTRACT

Adipic acid production may account for 10% of the annual increase in atmospheric nitrous oxide level. Here we developed a hollow $\text{H}_2\text{WO}_4/\text{TS-1}$ bifunctional catalyst with excellent catalytic activity for the direct transformation of cyclohexane to adipic acid with 30% hydrogen peroxide by a non- HNO_3 route. XRD diffraction, N_2 physisorption, TEM, NH_3 -TPD and Raman, XPS, Infrared, and UV-visible spectroscopies were used to characterize catalysts to increase understanding of the structure of active species on the hollow TS-1 support. The enhanced catalytic activity in comparison of reference catalysts (H_2WO_4 , $\text{H}_2\text{WO}_4/\text{Silicate-1}$ and TS-1) was explained in terms of their bifunctional catalytic sites and perfect hollow morphology with large intraparticle voids. Experimental results on the product distribution indicated that the tetrahedral Ti and surface W sites played important roles in the synergistic effect: tetrahedral Ti worked in oxidation of cyclohexane to intermediates (cyclohexanone and cyclohexanol) and surface W worked in further oxidation of late intermediates to adipic acid. Theoretical calculation results on catalytic activity of the Ti—O—O—H and W—O—O—H active sites in the $\text{H}_2\text{WO}_4/\text{TS-1}$ for different reaction steps validate the experimental results. The catalytic activity was also correlated to the strong interaction between W sites and HTS-1 surface induced increase in acidity of the materials. Increasing calcination temperature led to structural evolution of supported active species and subsequent activity change. A cyclohexane conversion of 31% with 78% adipic acid selectivity was achieved over this catalyst calcinated at 500 °C. Based on the catalytic and characterization results, possible reaction pathways were thus proposed to explain high adipic acid yield over hollow $\text{H}_2\text{WO}_4/\text{TS-1}$ catalysts.

© 2016 Elsevier B.V. All rights reserved.

1. Introduction

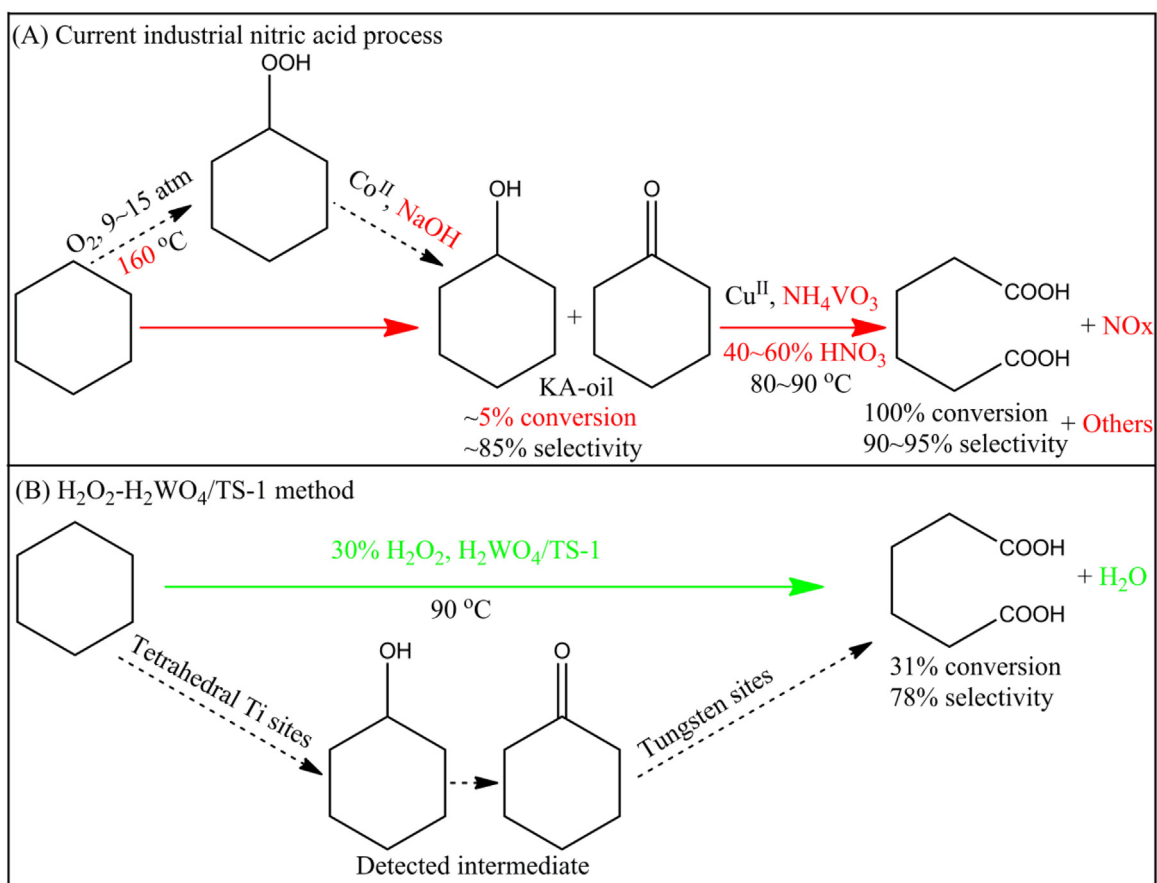
The development of green strategies for efficient production of industrial bulk chemicals is one of the most fascinating areas of research for the sustainability of human society [1]. Adipic acid (AA), as one of the most important dicarboxylic acids industrially, is used primarily for the large-volume manufacture of nylon-6,6 polymer [2,3]. In 2013, more than 3.5 million metric tons of AA were produced, reflecting a ~5% growth rate per year over the past 5 years [4]. The current commercial AA is mainly produced through the petroleum-based cyclohexane route which is carried out in two-stages (Scheme 1). The biggest challenge of the first stage is the difficulty in controlling the selectivity to KA-oil (a mixture of cyclohexanone and cyclohexanol) intermediate [5]. For example, to

obtain the desired KA oil, a low conversion of less than 5% is preferentially required by preventing the deep oxidation to by-products and reaction process consumes a large amount of NaOH leading to environmental pollution and increasing costs. In the second stage, the KA oil is rather inefficiently converted to AA by 40–60% HNO_3 in the presence of homogeneous vanadium-containing catalysts, causing large energy consumption and emission of significant amounts of environmentally harmful nitrous oxides (N_2O , NO, and NO_2). Adipic acid production may account for some 10% of the annual increase in atmospheric nitrous oxide level [6,7]. Among these nitrous oxides, N_2O constitutes the major source of polluting species, which is commonly thought to involve in both ozone depletion and the greenhouse effect [8,9]. Therefore, the direct conversion of cyclohexane into AA using molecular oxygen or H_2O_2 has been sought in pursuit of the goal of 'green chemistry'.

Many attempts have been made to develop more efficient and environmentally benign methods for industrial synthesis of AA that avoids the emission of N_2O . Molecular oxygen has

* Corresponding authors.

E-mail addresses: zwenz79@163.com (W. Zhong), mlq1010@126.com (L. Mao).



Scheme 1. Comparison of current industrial process and green method presented herein for production of AA.

been designed for oxidation of cyclohexane or cyclohexanone over $\text{Mn}(\text{OAc})_2/\text{Co}(\text{OAc})_2$ [10], μ_3 -oxo-bridged Co/Mn cluster complexes [11], Anderson-type polyoxometalates [12], microporous FeAlPO-31 [13] Mn/HTS-1 [14], and manganese porphyrins [15]. For example, Chavan et al. studied μ_3 -oxo-bridged Co/Mn cluster complex as a catalyst to convert cyclohexanone to AA in acetic acid medium with a selectivity of 86% [11]. Thomas and coworkers reported a direct, liquid-phase, catalytic oxidation of cyclohexane to AA over microporous FeAlPO-31 (selectivity of AA = 31.3% at cyclohexane conversions of 7.7% and 1.5 MPa) [13]. Apart from low conversion and drastic reaction conditions such as strong acid medium and high pressure used for cyclohexane or cyclohexanone oxidation using molecular oxygen, they also have significantly low selectivity for AA, as many over-oxidation products (succinic acid, glutaric acid, valeraldehyde, valeric acid and CO_x) are obtained.

Syntheses starting from cyclohexanone, cyclohexanol and cyclohexene to AA with H_2O_2 as an oxidant were actually widely considered to be one of the green synthetic processes. H_2O_2 has a high content of 'active' oxygen, and water is the only theoretical byproduct; this oxidant is cheaper and safer to use than the other peroxides, and in fact is produced in quantities of ~2.4 million metric tons per year for use [16–18]. In 1998, Sato et al. demonstrated a biphasic catalytic system using 30% H_2O_2 to convert cyclohexene to AA in the presence of a homogeneous Na_2WO_4 catalyst and the phase-transfer catalyst $[\text{CH}_3(n\text{-C}_8\text{H}_{17})_3\text{N}]\text{HSO}_4$ [19]. Several other tungstate-based catalysts such as peroxotungstate [20], silver supported tungsten oxide [2] and silica-functionalized ammonium tungstate [21] and $\text{Na}_2\text{WO}_4/\text{H}_3\text{PO}_4$ [22] have also been reported to be active for cyclohexene oxidation. In addition, many researchers came forward to produce AA by oxidation of cyclohexanone or cyclohexanol using H_2O_2 over materials based on H_2WO_4

[23] and phosphomolybdic heteropolyacids (HPAs) [24] as catalysts. Although the overall adipic acid yield (90%) is very high, the low availability of the substrates such as cyclohexene, cyclohexanone and cyclohexanol restricted the industrial application of these new developments. Thus, an environmentally friendly, yet practical route to AA from cyclohexane using cheap oxidants such as 30% H_2O_2 is highly desirable.

Titanium silicalite-1 (TS-1) with MFI structure has been found to catalyze a variety of synthetically important oxidations with an aqueous solution of H_2O_2 under mild conditions [25,26]. Examples include alkene epoxidation, alkane oxidation, phenol hydroxylation and cyclohexanone ammoxidation with $\text{H}_2\text{O}_2/\text{NH}_3$. Among the alkane oxidation reaction, cyclohexane oxyfunctionalization to KA-oil catalyzed by TS-1 has also been extensively studied showing that TS-1 can exhibit remarkably high efficiency and KA-oil selectivity, which is believed to be a 'green' route to substitute for old ones [27]. Following Spinacé's pioneer work with the TS-1 catalyst, Shi has reported a kind of hollow-structured TS-1 catalyst (HTS-1) for use in the oxyfunctionalization of cyclohexane and showed to be more active than solid-structured TS-1 with 30% H_2O_2 as oxidant [28]. It was proposed that the enhancing of dimensions of the intra-particle pores in structure can intensify the transport of reactants and products in and out of the crystal's channels. Recent studies from our laboratory have shown that the hollow-structured titanasilicate by implanting transition metal Mn ions in high oxidation states is more adapted for the production of bulky AA compared with cyclohexanol or cyclohexanone [14]. Further, this material also displays superior catalytic activity and selectivity in the oxidation of cyclohexanone to AA with molecular oxygen under mild solvent-free and promoter-free conditions [29]. The hollow nature of the catalyst with large intra-particle voids is believed to facilitate the

diffusion of bulky reaction intermediates (cyclohexyl hydroperoxide, ketonyl radical complex) to the internal catalytic site and increases the catalyst activity. Building on our prior experience with hollow-structured TS-1 and the work of Sato et al. (who used tungstic acid as catalyst to catalyze cyclohexanone or cyclohexanol to AA with H_2O_2 [23]), we design a novel H_2WO_4 /HTS-1 bifunctional catalyst with tetrahedral Ti species for activity of C–H bonds of cyclohexane and surface tungsten species for cleavage of later intermediates (KA oils), which is capable of catalyzing direct oxidation of cyclohexane to AA by 30% H_2O_2 (Scheme 1).

In present work, to understand the reaction mechanism and achieve direct oxidation of cyclohexane to AA, we characterized and tested a series of hollow-structured H_2WO_4 /HTS-1 bifunctional catalysts, in which, the tetrahedral Ti species in structure act as the activity components for cyclohexane oxidation to KA oil intermediates, while tungsten sites on the surface of HTS-1 play vital roles in the C–C cleavage of KA oil intermediates to AA. To further elucidate the role of each active site in the direct transformation of cyclohexane to AA, the data on the catalytic performance of H_2WO_4 , H_2WO_4 /Silicate-1 and HTS-1 are presented as well. In addition, the structural evolution of tungsten sites with calcination temperature is studied, and is well correlated with the catalytic property changes. This work not only provides insights into the structure and reactivity of active sites in H_2WO_4 /HTS-1 bi-functional catalyst and reaction mechanisms, but also gives a unique avenue toward further design of better catalysts.

2. Experimental

2.1. Catalyst preparation

The hollow-structured TS-1 was synthesized under hydrothermal condition by a dissolution-recrystallization process in tetrapropylammonium hydroxide (TPAOH) solution [29]. First, tetraethyl orthosilicate (TEOS), titanium butoxide (TBOT), TPAOH solution and distilled deionized water were mixed in a 1:0.01:0.4:40 molar ratio forming a clear solution, which was hydrolyzed for 2 h at 60 °C. The obtained gel was transferred to a Teflon-lined stainless steel autoclave and crystallized at 170 °C for 3 days. The white solid was filtrated and washed with large amounts of deionized water and dried at 120 °C for 24 h, followed by calcination at 500 °C for 10 h to remove the residual structure directing reagent. Secondly, the obtained solid TS-1 was treated with H_2SO_4 solution (a weight ratio of the previous calcined TS-1: H_2SO_4 :water = 10:1.2:140), and the acid-treated solid TS-1 was dispersed in TPAOH solution (a weight ratio of molecular sieve:TPAOH:water = 10:1.5:125). The mixture was then recrystallized in a Teflon-lined stainless steel autoclave at 140 °C for 3 days. Filtration of the recrystallized zeolite was washed, dried and finally calcined at 500 °C for 10 h. Silicate-1 was also prepared by an identical procedure, merely without adding titanium.

The hollow-structured H_2WO_4 /TS-1 catalysts were prepared by a simple ball milling treatment procedure. For each sample, 1.0 g hollow-structured TS-1 with the different amounts of H_2WO_4 was added into an agate tank. The ball milling was performed at 150 rpm for 1 h, followed by calcination at 500 °C in air for 4 h (with heating rate 5 °C/min). By changing the amount of H_2WO_4 powder, the hollow-structured W/TS-1 composites with 15, 25, 50 and 70 wt.% of H_2WO_4 were synthesized, labeled by 15% W/HTS, 25% W/HTS, 50% W/HTS and 70% W/HTS, respectively. For comparison, the catalyst 50% W/HTS was also calcined at 150, 300, 500 and 650 °C. Na_2WO_3 and the hollow-structured TS-1 were treated by the ball-milling method (labeled by 50% W/HTS(Na)) and the subsequent procedures were the same as those of W/HTS. W/Silicate-1 and

W/TS-1 were also prepared by an identical procedure with using Silicate-1 and solid-structured TS-1 as a support, respectively.

2.2. Characterization techniques

The crystalline phase of sample was checked by a Bruker D8 ADVANCE diffractometer operated at 40 kV and 40 mA with $\text{Cu}_{K\alpha}$ radiation ($\lambda = 1.542 \text{ \AA}$). Particle morphology of samples was studied using scanning obtained on a Hitachi S-4800 microscope, while the TEM images were recorded in a JEOL-JEM-2100 microscope operated at 200 kV. The BET surface area and porosity of samples were measured by N_2 adsorption at liquid N_2 temperature on a Tristar 3000 sorptometer. Prior to the measurement, the samples were degassed at 200 °C for 3 h. Raman spectra for the power samples were obtained on a Renishaw in Via Raman Microscope system with a 514.5 nm laser as the excitation source. A laser output of 30 mW was employed and the maximum incident power at the sample was approximately 6 mW. Framework infrared spectra of KBr pellets were recorded on an AVATAR 370 Thermo Nicolet spectrophotometer with a resolution of 2 cm^{-1} . UV/Vis diffuse-reflectance spectra were recorded on a Varian-Cary 5000 spectrometer with an integrating-sphere attachment to assess the nature of Ti and W species. BaSO_4 was used as background standard. The surface electronic states were analyzed by X-ray photoelectron spectroscopy (XPS, Axis Ultra, Kratos Analytical Ltd.) with Al K α radiation (1486.7 eV). The binding energies ($\pm 0.2 \text{ eV}$) were referenced to the C_{1s} peak at 284.8 eV. Fit XPS software was used for curve fitting.

2.3. DFT calculations

The geometrical structures of the smallest models with active sites, TiO_6H_6 (a) and WO_6H_3 (b), were optimized using a LANL2DZ basis set for W and Ti and a 6-311+G(d, p) basis set for all other atoms. Similar computational methods have been shown to yield accurate geometries for similar titanium and tungsten species [30,31]. All the calculations were performed with the Gaussian 09 program, to gain insight into the electronic distribution and bonding distances of peroxo active sites. In both models, the unsaturated bonds were saturated by hydrogen atoms.

2.4. Catalytic oxidation of cyclohexane to AA

Liquid phase oxidation of cyclohexane with 30% H_2O_2 as oxidant was carried out in a Teflon-lined 100 mL stainless-steel autoclave equipped with a magnetic stirrer. Typically, 2.1 g of cyclohexane, 4.2 g of 30% H_2O_2 aqueous solution, 15 g of acetone and 0.1 g of catalyst were charged to the autoclave in one lot, the autoclave was closed and submerged a thermostatically controlled oil bath at reaction temperature for different periods of time. After the reactions, the reaction mixture and catalyst were separated by filtration. The components of liquid phase such as unreacted cyclohexane, cyclohexanone and cyclohexanol were identified by GC–MS and quantitatively analyzed by an Agilent 6890 N GC with a $30 \text{ m} \times 0.32 \text{ mm} \times 0.50 \text{ }\mu\text{m}$ DB-17 polysiloxane capillary column and FID using *n*-hexanol as an internal standard. Both the injector and detector temperature were 250 °C, and the column temperature was 100 °C. The AA and overoxidation products (succinic acid, glutaric acid and valeric acid) were identified by HPLC–MS and by comparison with commercially pure products. These acidic products were quantitatively analyzed by an Agilent 1100HPLC equipped with a UV detector (212 nm, Agilent G1365B MWB) and a column of Zorbax Eclipse XDB C18 ($150 \text{ mm} \times 4.6 \text{ mm i.d.}$) using heptane diacid as an internal standard. The eluent was $0.01 \text{ mol L}^{-1} \text{ KH}_2\text{PO}_4$ in a 1:9 methanol/water mixture and a flow rate set at 1.0 mL/min . The components of oxygen formed were analyzed by

gas chromatography with TCD detector. The products were satisfactorily identified by comparing the MS spectra with those of the authentic samples. The amount of H_2O_2 consumed (H_2O_2 cons.) was determined by iodometric titration of the unreacted portion. Mass balances were verified. *Caution!* The oxidation reactions in acetone using hydrogen peroxide are necessary care and safety precautions should be taken.

3. Results and discussion

3.1. Characterization of the catalysts

3.1.1. Crystal structure and textural property

The XRD patterns of the un-modified and H_2WO_4 -modified HTS catalysts, with the pure H_2WO_4 are shown in Fig. 1A. The characteristic MFI diffraction peaks for the HTS-1 support are present at 7.95° , 8.94° , 23.2° , and 24.1° , which correspond to the indices of the [101], [200], [501], and [303] planes [32]. After the amount of H_2WO_4 was loaded on the HTS-1, the corresponding intensities of MFI diffraction peaks decrease and diffraction peaks are slightly broadened due to the coverage of the external surface of HTS with tungsten species. Additionally, the MFI diffraction peaks of H_2WO_4 -modified HTS-1 catalysts are shifted to the lower angle side compared with that of the pure HTS-1, which can be due to the interaction between the tungsten species and HTS-1 support. The detailed analysis of the XRD patterns for W/HTS with 50% H_2WO_4 loading shows new sharp peaks at 2θ values of 23.1° , 23.5° , 24.4° , 33.4° and 34.2° (JCPDS 43-1035), confirming the formation of WO_3 crystallites. This indicates low content of tungsten species in HTS may be partly incorporated into the framework of zeolite or homogeneously dispersed on the surface of the zeolite. Compared with the H_2WO_4 , it is interesting to mention here that the new XRD peaks of W/HTS catalysts is not matching exactly with WO_3 crystallite peaks, indicating a mixture of different phases of tungsten oxide species. To verify the structural evolution of tungsten oxide species, 50% H_2WO_4 -modified HTS-1 catalysts after heat treatments in air at different temperatures shown in Fig. 1B are also characterized by XRD. For heat treatment at temperatures 150°C or lower, two strong peaks similar to pure H_2WO_4 are observed in the XRD pattern, indicating that no decomposition of H_2WO_4 is observed in the samples. The oligomeric W species condense and crystallize only after heat treating to 300°C and above as suggested by the well-defined diffraction peaks. The intensity of crystalline WO_3 formed increases with further increasing calcination temperature, suggesting that the crystallite size increases by condensation of isolated small $(\text{WO}_3)_n$ clusters species between neighboring WO_x groups; additionally the peak intensities of the corresponding reflections progressively increase with the H_2WO_4 loading.

The hollow structure and textural properties of HTS-1 and H_2WO_4 -modified HTS-1 catalysts are studied by N_2 sorption analysis (Fig. 2). For pure HTS-1, the presence of intra-crystalline voids accessible only via entrances smaller than 4 nm is evident from abrupt closure at $p/p_0 = 0.42$ on the desorption branch and differ from those of traditional TS-1 [33,34]. After loading with H_2WO_4 , they still display similar Type IV isotherms with a H2 hysteresis loops, indicating the presence of intra-crystalline voids same as the pure HTS-1 (Fig. 2A). But the over-loading of H_2WO_4 to HTS (70% W/HTS) leads to a drastic decrease of N_2 quantity adsorbed due to the possible blocking or covering of the intra-crystalline voids in HTS-1. The sharp BJH pore size distribution curves shown in Fig. 2B also confirm the hollow structure of HTS-1 and H_2WO_4 -modified HTS-1 catalysts; additionally, the width of the intra-crystalline voids of HTS-1 and H_2WO_4 -modified HTS-1 centers at 3.1 nm. Thus, the well-defined hollow structure with a higher content of tungsten species can overcome pore diffusion limitations and facilitate

bulky molecular transport to more absorption and/or reacting sites for cyclohexane oxidation, resulting in a higher catalytic activity.

The micro-structure and morphology of catalysts are studied with TEM. The large intraparticle voids with an average particle size of 150–250 nm can be seen in TEM image of HTS-1 in Fig. 3A₁, and the large voids are located exclusively in the inner part of the crystals and never communicate directly with the surface (3A₂ and 3A₃). This phenomenon indicates that the dissolution-recrystallization process only affects essentially the core of the crystals by a gradient of defect sites throughout the crystals [35]. When H_2WO_4 was supported into HTS-1, the intra-crystalline voids remains intact (Fig. 3B₁ and 3B₂); additionally, the resulting W/HTS shows a similar morphology with hollow sphere-like structure to that of matrix HTS. Interestingly, from Fig. 3B₃, it can be seen that tungsten species in W/HTS mainly develop inside the voids of HTS. On the other hand, some agglomerated particles of WO_3 are also observed in W/HTS. In the enlarged TEM image (Fig. 3B₄), distinct crystal fringes with a spacing of 0.376 nm are observed, corresponding to d-spacing of tungsten oxide (010) crystal planes [36,37]. The TEM micrograph in Fig. 3B₄ also exhibits well-ordered lattice fringes of the MFI structure of TS-1 in the under right corner, which is indicative of high crystallinity. On the other hand, this also confirms that the pore array is regular and ordered without interruption on the [010] plane. Thus, the hollow structure exists in W/HTS predominantly between the unit cells along the b direction.

3.1.2. Surface characteristics and acidic property

UV-vis DRS is a sensitive tool for detection of framework incorporated metal and extra-framework metal oxide in different mesostructures [38,39]. For comparison, UV-vis DRS spectra of Silicate-1, HTS-1 and H_2WO_4 are also shown in Fig. 4A. UV-vis DRS spectra of HTS-1 and Silicalite-1 show that there is a typical absorption band centered at 210 nm for HTS-1, while no electronic absorption band is observed for Silicalite-1. The band at 210 nm is usually ascribed to a charge transfer of the $p\pi-d\pi$ transition between Ti^{4+} and O^{2-} of the traditional TS-1 framework titanium species [40,41]. Additionally, a small amount of anatase (330 nm) is also present [42], which may be attributed to the treatment with TPAOH by involving the dissolution-recrystallization of solid-structured TS-1. The recrystallization process can lead to the rearrangement of $[\text{TiO}_4]$ and $[\text{SiO}_4]$, which will saturate the tetrahedral-coordinated Ti and increased the content of the octahedral one. When compared with the pure HTS, UV-vis DRS spectra of W/HTS catalysts shown in Fig. 4A display an absorption band centered around 218 nm, which is attributed to ligand-to-metal charge transfer in isolated $[\text{WO}_4]^{2-}$ tetrahedral species [38]. The presence of a band around 270 nm is attributed to the charge transfer from O^{2-} to W^{6+} , confirming the existence of low condensed oligomeric W species with octahedral coordination [43]. The diffraction peak at 400 nm assigned to extraframework WO_3 is also observed [44], and the intensity increases with the increase of H_2WO_4 loading. This result is in accordance with that obtained by XRD and TEM.

The FT-IR technique is also an effective method for detection of framework Ti and W species. The FT-IR spectra (Fig. 4B) of both the HTS-1 composite and the Ti-free Silicate-1 show that the characteristic bands of MFI topology are sited at 450, 550, 800, 1110, and 1220 cm^{-1} [45]. These bands are commonly ascribed to a stretching vibration mode of Si–O–Si in SiO_4 units. Obviously, two characteristic bands at 530 and 960 cm^{-1} , not observed for pure Silicate-1, are usually assigned to the stretching vibration of Si–O in $(\text{Si}-\text{O})_3\text{Si}-\text{O}-\text{Ti}$ unit or that of $\text{Si}-\text{O}^{\delta-}\cdots\text{Ti}^{\delta+}$, being indicative of the insertion of Ti into the HTS-1 framework [46]. Together with the open framework structures with large intraparticle voids, the catalytic titanium site inside the voids of HTS-1 can efficiently catalyze the conversion of bulky cyclohexane to its corresponding KA-oil intermediates with O_2 . The FT-IR spectrum of the H_2WO_4 sam-

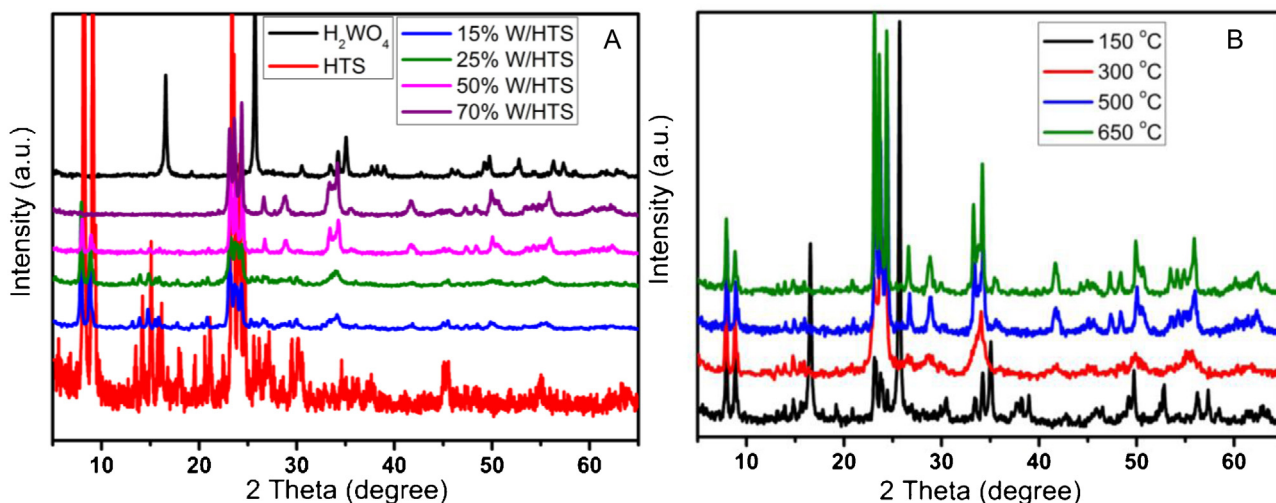


Fig. 1. XRD patterns of (A) samples (H₂WO₄, HTS-1, 15% W/HTS, 25% W/HTS, 50% W/HTS and 70% W/HTS) and 50% W/HTS sample calcined at different temperatures (B).

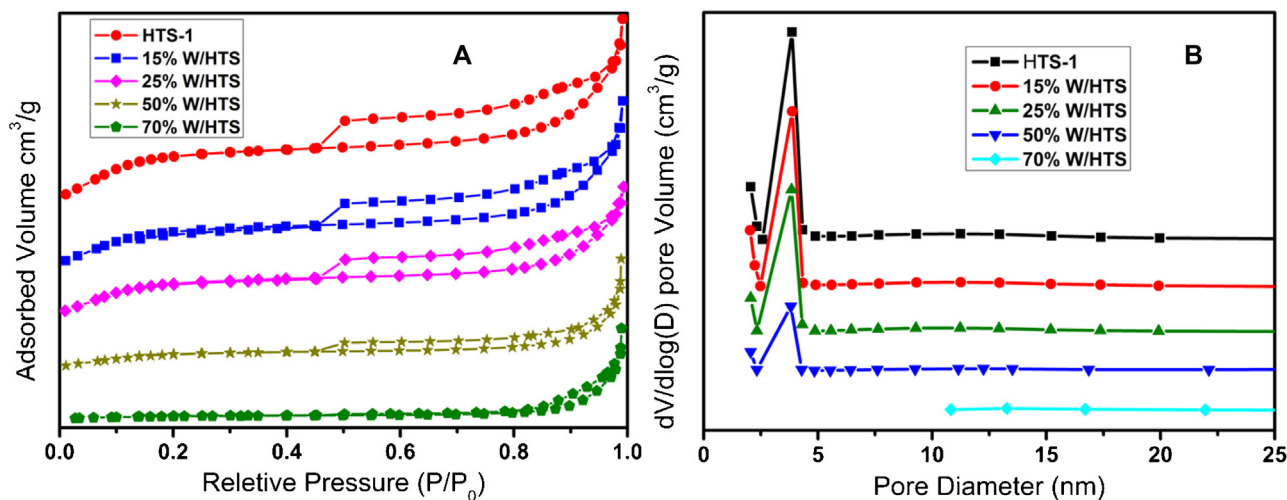


Fig. 2. N₂ adsorption-desorption isotherms (A) and pore diameter distribution (B) of samples (HTS-1, 15% W/HTS, 25% W/HTS, 50% W/HTS and 70% W/HTS).

ple diluted in KBr shows a broad band at 590–710 cm⁻¹ assigned to W–O–W, W–O–H, and W–O···HO–W stretch vibrations and a sharper band at 940 cm⁻¹ attributed to the W=O stretch [47]. The introducing of W species into the HTS-1 leads to a new band at 774 cm⁻¹ assigned to a stretching vibration mode of W–O–W bonded with the silicon [48]. The occurrence of this bands indicates the presence of W–O–Si bridge site in the W/HTS materials. Additionally, the position of the peak at 940 cm⁻¹ shifted to lower wave numbers (red shift) and the band shape becomes broader, which can be assigned to the presence of W=O groups side-on bound to the silicon (W=O–Si bonds) [49]. The stability of W species on HTS-1 is related to the strong W–O–Si and W–O–Si bonds between the tungsten species and the HTS-1 surface, as suggested by high oxidation temperatures of WO_x-ZrO₂ catalysts [50].

The major structural information concerning the surface tungsten species can be derived from Raman spectroscopy (Fig. 5) because of its ability of distinguishing different tungsten oxide that may simultaneously be present on the materials. In the Raman spectra of HTS-1 (Fig. 5A), the weak Raman band at 526 cm⁻¹ assigned to the symmetric stretching vibrations of the framework Ti–O–Si species in the local unit of [Ti(OSi)₄] [51], confirms the presence of framework titanium species in tetrahedral coordination as shown in expanded Fig. S1. The interesting bands at 148, 398, and

644 cm⁻¹ are also observed, indicating that there are extraframework titanium species in the HTS-1 material [33,34]. These are well in accordance with the UV–vis DRS absorption results. Obviously, the Raman spectra of W/HTS are completely different from that of HTS-1. The two strong Raman bands at 709 and 805 cm⁻¹, which appear for W/HTS, are absent in the Raman spectra of HTS-1 and H₂WO₄. On the other hand, the weak bands at 398, 526, and 644 cm⁻¹ disappear for W/HTS. These new bands at 709 and 805 cm⁻¹ corresponding to W–O stretching and bending may be from the small (WO₃)_n clusters in W/HTS [52]. As tungsten species surface density increases, the relative number of W–O bonds within (WO₃)_n clusters increases and WO₃ domains grow in size; additionally the new bands at 179, 268, and 327 cm⁻¹ are observed. The band at 268 cm⁻¹ assigned to a W–O–W deformation mode indicates that initial W–O–W bonds form by condensation of isolated small (WO₃)_n clusters species between neighboring WO_x groups as the surface area of the HTS-1 support decreases and the (WO₃)_n clusters surface density increases during oxidation treatments [50]. The formation of these W–O–W bonds between small (WO₃)_n clusters leads to larger domains and to a narrowing of the HOMO–LUMO gap, as shown in UV–vis DRS absorption. The bands at 179 and 327 cm⁻¹ can be attributed to a lattice vibrational mode of O–W–O for WO₃ [53].

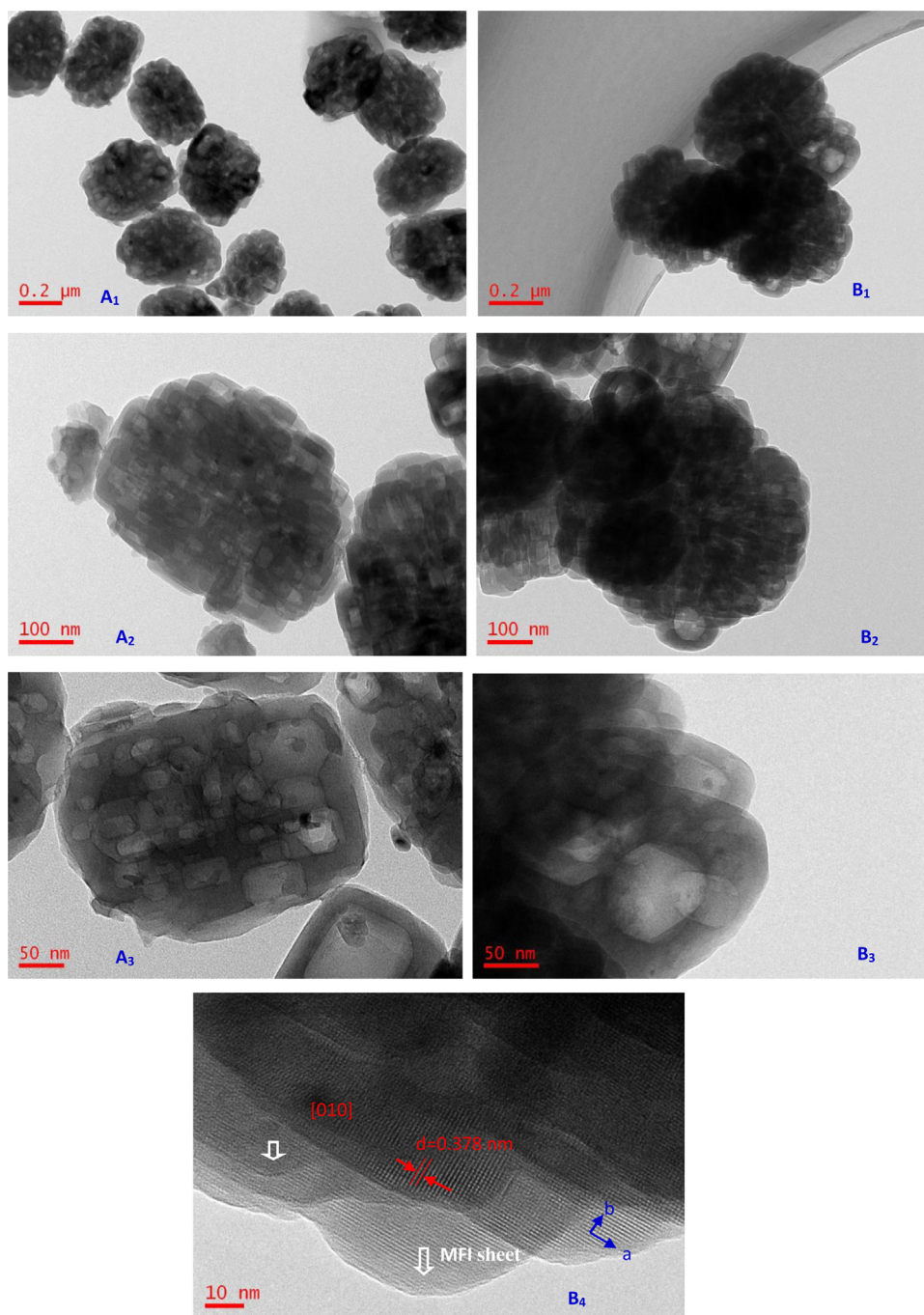


Fig. 3. TEM images of HTS-1 sample (A_1 , A_2 and A_3) and 50% W/HTS sample (B_1 , B_2 and B_3). Horizontal scale bars: A_1 and B_1 , 0.2 μm ; A_2 and B_2 , 100 nm; A_3 and B_3 , 50 nm; B_4 , 10 nm. The measured lattice distance 0.378 nm is indexed to d-spacing of tungsten oxide (010) crystal planes.

The evolution of the tungsten species in the W/HTS is followed by Raman spectra during the calcination of the W/HTS catalysts (Fig. 5A). The relative intensities of the bands at 179, 268, 709 and 805 cm^{-1} significantly increase with the calcination temperature. Additionally, these Raman bands, particularly the intensities of the bands at 709 and 805 cm^{-1} become stronger for higher calcination temperature, indicating that the more small $(\text{WO}_3)_n$ clusters eventually form W–O–W bridging bonds between neighboring WO_x groups in the W/HTS. The bands at 268 and 327 cm^{-1} develop with calcination temperature also strongly confirms this fact. The surface tungsten oxide species possessing some intermediate valence state and polytungstate structure, have a higher catalytic activity

for conversion of later KA oil intermediates to AA in the supported tungsten HTS-1 catalyst.

The acidic properties of the pure HTS-1 and H_2WO_4 -modified HTS-1 catalysts are studied by NH_3 -TPD analysis and the achieved results are shown in Fig. 6. The powdery HTS-1 only contains a few weak acid centers (<300 $^\circ\text{C}$), while 50% W/HTS shows two desorption peaks at both the weak acid center and strong acid center (>300 $^\circ\text{C}$) [54]. The strong acid centers are considered to be formed mainly by the incorporation of tungsten species on the surface. Furthermore, the surface concentration of weak acid center decreases, possibly due to that HTS surface is partly covered by the high dispersion of tungsten species in the 50 wt% HTS catalyst, indicating the presence of strong interactions between active tungsten species

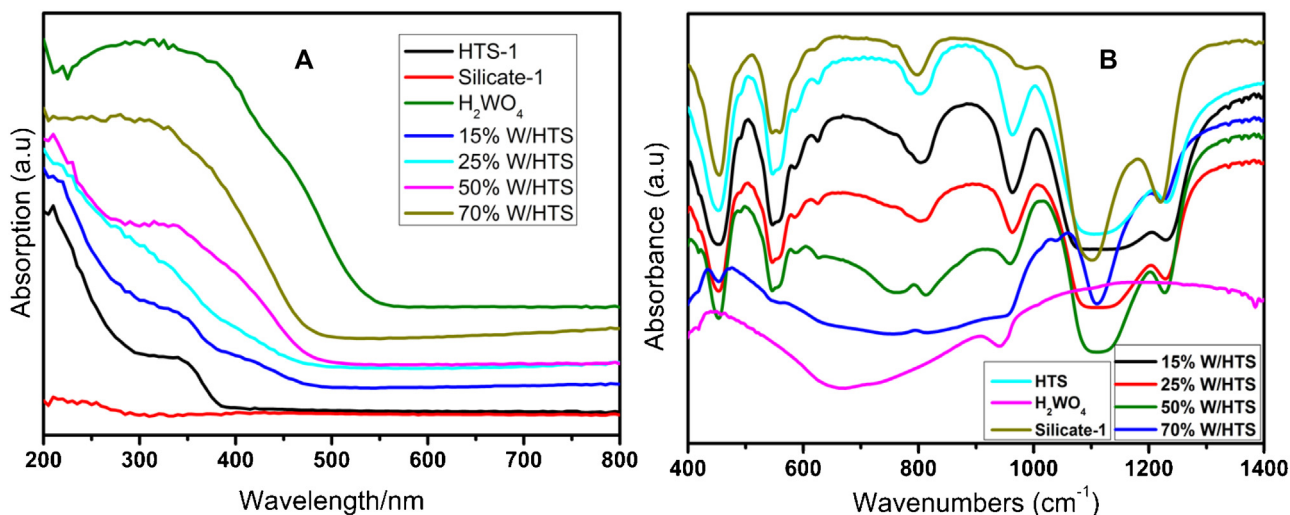


Fig. 4. UV-vis spectra (A) and FT-IR spectra (B) of samples (H_2WO_4 , Silicate-1, HTS-1, 15% W/HTS, 25% W/HTS, 50% W/HTS and 70% W/HTS).

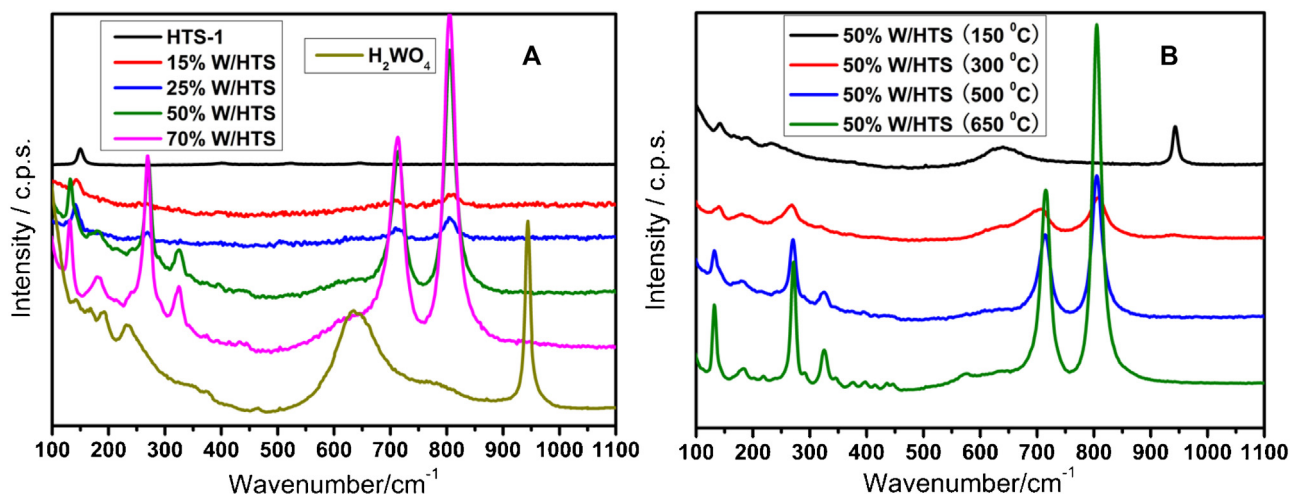


Fig. 5. Visible Raman spectra of (A) samples (H_2WO_4 , HTS-1, 15% W/HTS, 25% W/HTS, 50% W/HTS and 70% W/HTS) and 50% W/HTS sample calcined at different temperatures (B).

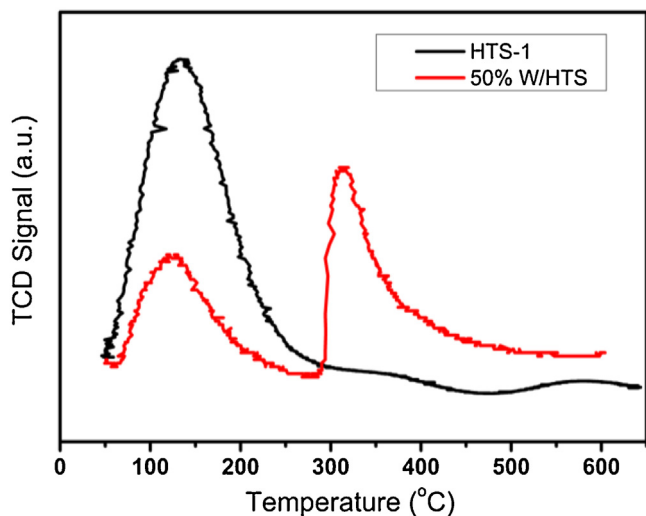


Fig. 6. NH_3 -TPD curves of samples (HTS-1 and 50% W/HTS).

and the silica-based matrix. The strong acid centers are essential to accelerate the tautomerism between cyclohexanone and the corresponding enolic form; thus, enolic form will be more easily activated by radical H abstraction than cyclohexanone itself to produce radical species in the oxidation of intermediate cyclohexanone [29].

3.1.3. Chemical state

XPS spectra are measured to investigate the chemical state of the elements present in W/HTS through the binding energy (BE). The XPS survey spectra of the H_2WO_4 -modified HTS-1 and pure HTS-1 zeolite are reported in Fig. 7. The H_2WO_4 -modified HTS-1 contains Ti, W, Si, O, and trace amounts of adventitious C, which may be attributed to impurities from the residual carbon in the pure HTS-1 zeolite (Fig. 7A). Based on the Ti 2p spectra shown in Fig. 7B, it is evident that the Ti 2p_{3/2} peak for the pure zeolite is found at the BE of ~ 460.1 eV belonging to the tetrahedral Ti in the HTS [55]. The peak for the H_2WO_4 modified pure HTS-1, however, displays a shoulder (with a fractional amount of 17%) at lower BE. From the slight positive shift to ~ 459.4 eV of the Ti 2p_{3/2} BE in the W/HTS, we can assume that part W species are incorporated into the lattice of HTS-1 and influence the local chemical state of Ti^{4+} ions. Furthermore, the Ti 2p region of W/HTS can be resolved into two

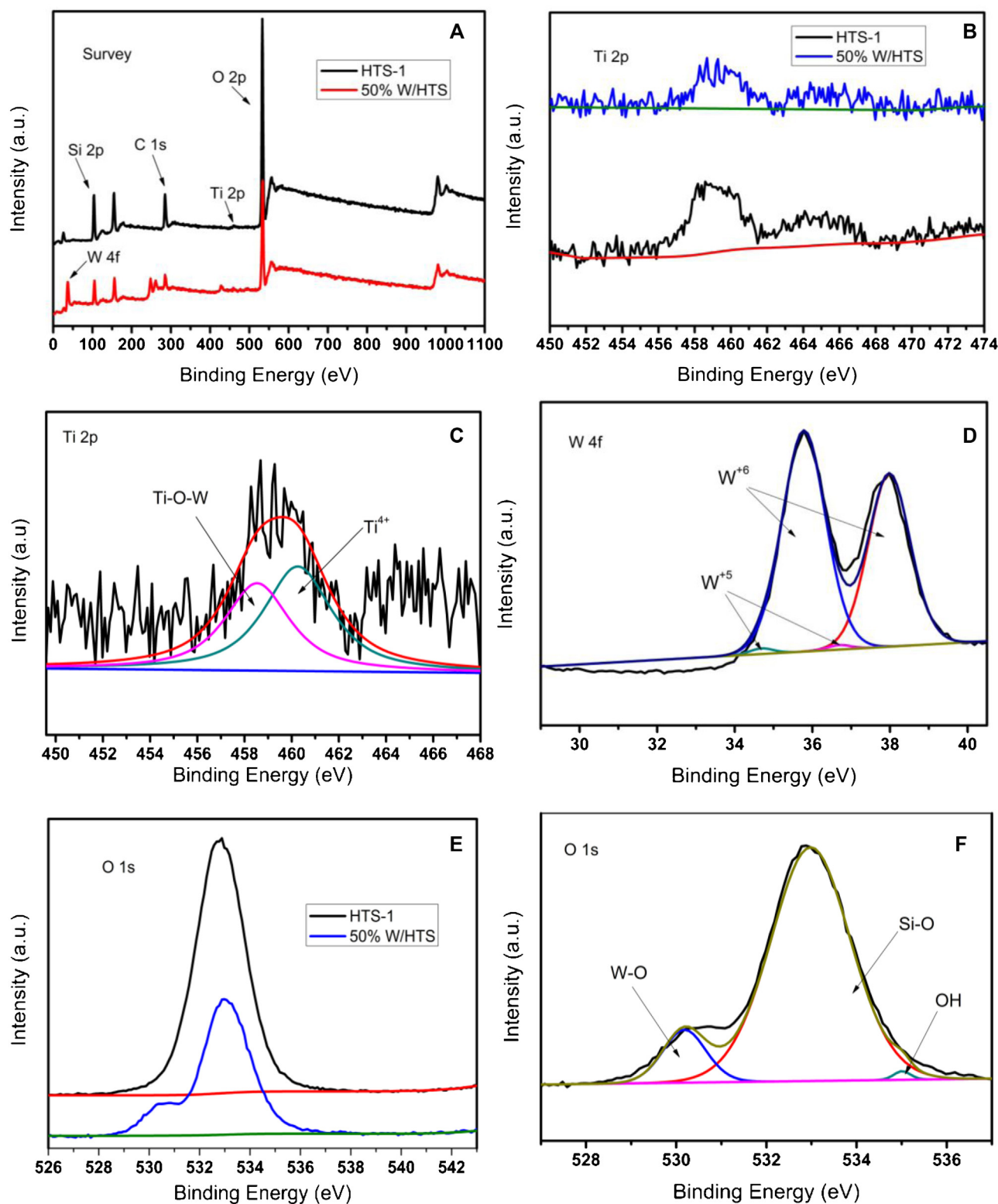


Fig. 7. Survey spectrum of samples (A) and XPS spectra of Ti 2p (B) and (C), W 4f (D) and O 1s (E) and (F) of samples (HTS-1 and 50% W/HTS).

parts according to the theory of Doniach and Sunjic (Fig. 8C) [56], the peak at 460.1 eV corresponds to Ti^{4+} species whereas the one at 458.6 eV is characteristic of Ti–O–W bridge located on the surface [53]. This can indicate the formation of Ti–O–W at the interface of the H_2WO_4 modified HTS-1 materials during the calcination.

Fig. 7D shows the W 4f core level spectrum of the W/HTS, and the measured spectrum can be deconvoluted into two doublets.

The first doublet has the BE of 37.9 and 35.8 eV belonging to W $4f_{7/2}$ and W $4f_{5/2}$ of W^{6+} species [57], respectively, while the second doublet with weak intensity has a lower BE of 36.7 and 34.6 eV corresponding to W $4f_{7/2}$ and W $4f_{5/2}$ of W^{5+} species [58], respectively. The shift to negative BE values for the W $4f_{7/2}$ and W $4f_{5/2}$ peaks for referenced values of WO_3 is due to the differences in electronegativity and polarizability of the elements. For example, Ti^{4+}

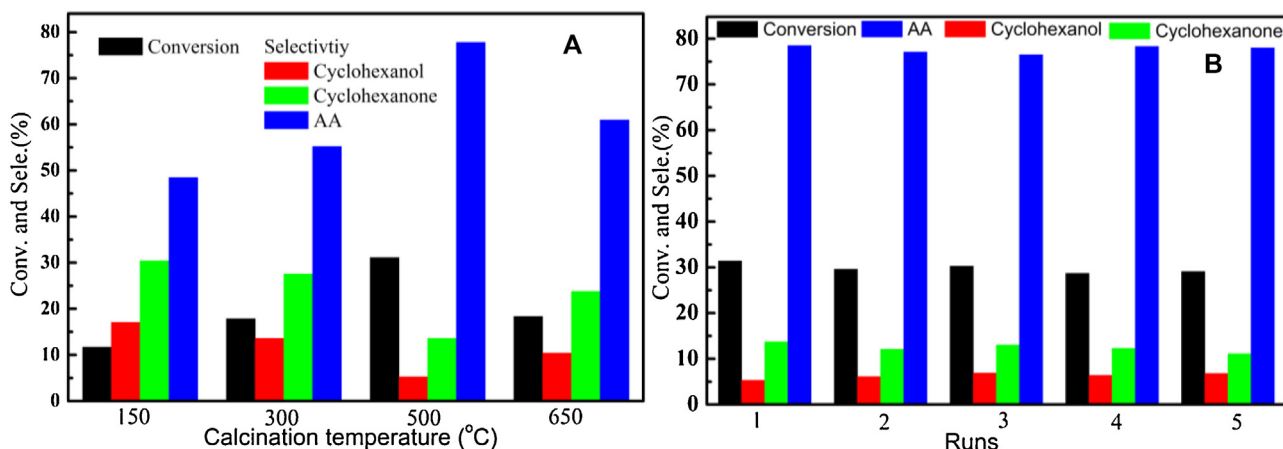


Fig. 8. Catalytic results on 50% W/HTS calcined at different temperature (A) and recyclability tests of 50% W/HTS catalyst for the cyclohexane oxidation (B). All reactions were done with 0.10 g of catalyst, 25 mmol cyclohexane, 30% H_2O_2 (75 mmol), 19 mL of acetone, at 90 °C, time (14 h).

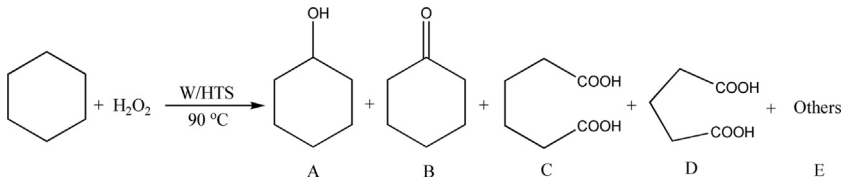
ionic radius (0.68 Å) is slightly larger than W^{6+} ions (0.62 Å), which allows for feasible electron cloud distortion and higher polarizability. Additionally, the different surface states of tungsten species of the interaction between W and Si through O bonding may be also existed in modified W/HTS, referring to the results reported by Hu et al. [49]. The appearance of W^{5+} species in modified W/HTS-1 catalysts may be due to the incorporation of W species into HTS-1 framework by the solid–solid reaction between W species and HTS-1 [59]. For modified W/HTS, the broad and asymmetric peak of O 1s in HTS-1 becomes two peaks (Fig. 7E). The O 1s region shown in Fig. 7F is further fitted with three parts, one at 532.9 eV originating from Si–O band, the second at 530.2 eV resulting from the formation of W–O band [60], and the third at 534.9 eV corresponding to –OH species.

3.2. Catalytic performance of the catalysts

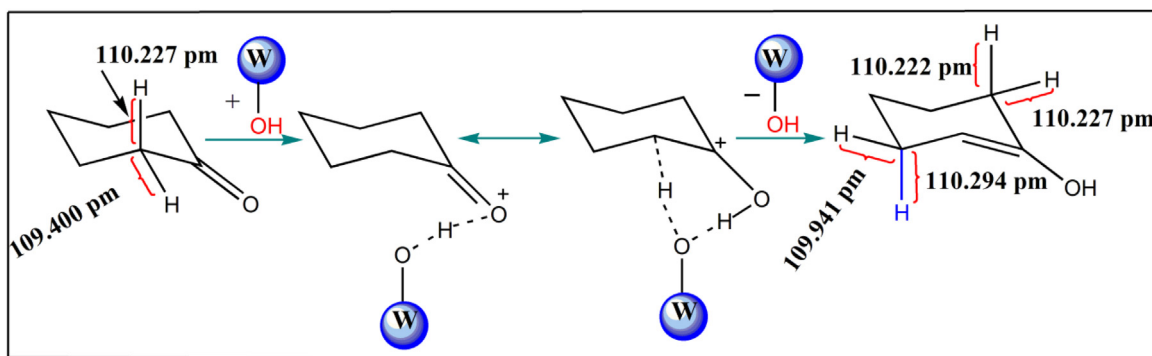
Direct oxidation of cyclohexane to AA with 30% H_2O_2 over the as-synthesized materials was evaluated in a batch-type stainless steel reactor at 90 °C for 14 h and compared with the pure HTS-1 and H_2WO_4 , as shown in Table 1. As expected, the blank experiment without any catalyst shows that only 3.7% of H_2O_2 is decomposed and that only very small amounts of KA oil are formed, as a result of the abstraction of H atom by $\cdot\text{OH}$ radicals produced in the thermal decomposition of H_2O_2 (entry 1). The hollow HTS-1 material is active for the cyclohexane oxidation and a cyclohexane conversion of 38.2% was obtained (entry 2). Cyclohexanone is the main product (66.4%) along with cyclohexanol (30.5%), whereas AA is formed with very low selectivity (1.7%). In marked contrast, AA became the predominant product (78.5%) and cyclohexanone and cyclohexanol selectivities were very low (13.7 and 5.3%, respectively) when H_2WO_4 -modified HTS-1 was used instead of pure HTS-1 (entry 7). As a result, cyclohexane conversion and intermediate KA oil selectivity are correlated with the nature of the Ti–O_x species existing in a tetrahedral coordination (Ti–O₄ species), which preserves a larger fraction of the primary KA oil intermediates in the reacting mixture. Since the Ti–O₄ species show a very low activity for the formation of AA (1.7%), the W species in the HTS are responsible for the C–H bond activation of cyclohexanone and/or cyclohexanol and then react in subsequent reactions with H_2O_2 to form AA. Therefore, H_2WO_4 and H_2WO_4 -modified Silicate-1 were further investigated for cyclohexane oxidation as a possible reference, respectively (entries 3 and 9). Low catalytic activity, however, was obtained under similar conditions. This appears to reflect the lower reactivity of W species for first reactions of cyclohexane to form KA oil intermediates compared with Ti–O₄ species on HTS surfaces.

To further verify the role of Ti–O₄ and W species, two compared separate experiments have also been tested, the first one is investigated with the addition of cyclohexanol and cyclohexanone instead of cyclohexane over the pure HTS-1 catalyst, respectively (entries 11 and 12). The oxidation productions of cyclohexanol are cyclohexanone (89.2%) and AA (2.8%); cyclohexanone oxidation reaction produces AA (32.3%) and glutaric acid (18.4%), giving a total of 4.7% cyclohexanone consumed. In fact, these products with the similar compositions for cyclohexanone oxidation were formed by the uncatalyzed reaction (not shown). These results indicate that cyclohexanol is readily oxidized to cyclohexanone and ‘over-oxidation product’ while cyclohexanone is very slowly ‘over-oxidized’ on the Ti–O₄ sites. While in the second experiment, the oxidation of cyclohexanol and cyclohexanone instead of cyclohexane over the H_2WO_4 -modified Silicate-1 was also tested, respectively; it’s found that the high AA yields were obtained for cyclohexanol and cyclohexanone (entries 13 and 14). In addition, we also measured the catalytic activity of W/TS-1 in the oxidation of cyclohexane under the same conditions. It is found that 21.4% adipic acid selectivity with cyclohexane conversion (10.3%) was obtained in the oxidation cyclohexane experiment (entry 11), indicating that the hollow structure of W/HTS can overcome pore diffusion limitations and facilitate bulky molecular transport to more absorption and/or reacting sites for direct oxidation of cyclohexane to adipic acid, resulting in a higher catalytic activity.

The identity of surface strong acidic sites of the W/HTS catalyst influences conversion and AA selectivity, a Na_2WO_4 -modified HTS-1 catalyst was measured (entry 10). Na_2WO_4 precursors supported on HTS-1 were less reactive for KA oil intermediates oxidation than H_2WO_4 -modified HTS-1 because of structural degradation of Na_2WO_4 on HTS-1 to form WO_x species without surface strong acidic sites domains, which indicated that the surface strong acidic nature of the catalyst is crucial for the reaction. A similar acceleration effect of H_2WO_4 catalysts (compared with Na_2WO_4), although has been already reported in the oxidation of cyclohexanone or cyclohexanol with aqueous 30% H_2O_2 in the past decade (H_2WO_4 is also readily oxidized with H_2O_2 to form $\text{H}_2[\text{WO}(\text{O}_2)_2(\text{OH})_2]$), has almost never been considered [23]. Based on the different configurational isomers of the cyclohexanone (keto-form and enol-form) by our DFT investigation [29], calculation results show that the C–H bond distance of the enol-form connecting a double bond (110.294 pm) is larger than one of the C–H bond distance of the keto-form connecting the carbonyl group (110.227 pm). Thus it was more easy for homolytic cleavage of the longer C–H bond of enol-form isomers. Therefore, a possible explanation for this effect is that surface strong acidic sites of the catalyst can accelerate the tau-

Table 1Direct oxidation of cyclohexane to AA with 30% H₂O₂ catalyzed by W/HTS catalysts^a.


Entry	catalyst	H ₂ O ₂ Eff. ^b (%)	Conv. ^c (%)	Selectivity ^d (%)				
				A	B	C	D	E
1	blank	7	0.4	34.1	32.6	3.1	2.2	28
2	HTS-1	68	38.2	30.5	66.4	1.7	0.8	0.6
3	H ₂ WO ₄	51	3.5	11.9	31.8	56.3	—	1.4
4	Silicate-1	9	0.6	31.7	35.9	2.6	3.8	26
5	15% W/HTS	66	35.6	33.1	45.5	21.4	—	—
6	25% W/HTS	61	34.1	16.8	37.6	45.6	—	—
7	50% W/HTS	53	31.4	5.3	13.7	78.5	1.4	1.1
8	70% W/HTS	27	11.2	5.4	28.2	33.6	26.3	6.5
9	50% W/Silicate-1	53	3.8	9.9	27.8	50.3	2.7	9.3
10	50% W/HTS(Na)	14	17.3	23.7	76.3	18.0	1.8	2.6
11	50% W/TS-1	57	10.3	19.1	28.2	21.4	21.6	9.7
12 ^e	HTS-1	71	91.0	—	89.2	2.8	—	8.0
13 ^f	HTS-1	23	4.7	—	—	32.3	18.4	49.3
14 ^e	50% W/Silicate-1	76	67.1	—	20.5	70.4	7.9	1.2
15 ^f	50% W/Silicate-1	83	87.0	—	—	92.6	6.1	1.3
16 ^g	50% W/HTS	—	1.3	34.2	22.6	18.4	11.8	13
17 ^h	50% W/HTS	—	3.2	—	—	68.3	12.5	19.2

^a All reactions were done with 0.10 g of catalyst, 25 mmol cyclohexane, 30% H₂O₂ (75 mmol), 19 mL of acetone, at 90 °C, time (14 h).^b The efficiencies of H₂O₂ (H₂O₂ eff.) were calculated taking into account that 1 mol of H₂O₂ is needed to produced 0.5 mol of cyclohexanone, 1 mol of cyclohexanol, or 0.2 mol of AA.^c Conversion (%) based on substrate = {1 - [(concentration of substrate left after reaction) × (initial concentration of substrate) - 1]} × 100.^d Product selectivity = content of this product / (adding cyclohexane amount (mmol) - the amount of cyclohexane recovered (mmol)) × 100%; Others: 2-hydroxycyclohexanone, 4-hydroxycyclohexanone and 1,2-cyclohexanedione, ε-oenantholacton and succinic acid.^e Using cyclohexanol (25 mmol) instead of cyclohexane.^f Using cyclohexanone (25 mmol) instead of cyclohexane.^g Addition of hydroquinone as a free radical scavenger (5 mol% cyclohexane).^h Addition of hydroquinone as a free radical scavenger (5 mol% cyclohexanone).**Scheme 2.** The activation of cyclohexanone via protonation and tautomerisation.

omerism between cyclohexanone and the corresponding enolic form, which is more easily activated by radical H abstraction than cyclohexanone itself to produce radical species (Scheme 2).

Based on the above characterization results, increasing H₂WO₄ loading and calcination temperature can lead to structural evolution of supported tungsten species. To elucidate whether the nature and structure of the tungsten species are a key factor in determining the catalytic performances, H₂WO₄ loading on the W/HTS materials are first considered (Table 1, entries 5–8). It was found that with increasing H₂WO₄ loading, although the conversion decreases, the AA selectivity increases. The catalyst with 50 wt% H₂WO₄ loading exhibited the best performance with a cyclohexane conversion of 31.4% and AA selectivity of 78.5%, which indicated that poly-tungstate structure and the terminal W=O group in the WO₃

crystallites are catalytic active sites. Further increasing the content of H₂WO₄ loading to 70%, nevertheless, lowered the cyclohexane conversion. This may be due to the fact that most of voids on the intra-crystalline are blocked by tungsten species (as observed by N₂ sorption analysis) and limits bulky molecular transport to more absorption and/or reacting sites. For this reaction, the diameter of reactant cyclohexane is 0.49 nm (the distance between hydrogen and the most distant hydrogen is 0.47 nm; the van der Waals radius of hydrogen is 0.10 nm) and that of the products cyclohexanol, cyclohexanone and AA should be 0.58, 0.51 and 1.0 nm, respectively, while the average pore diameter for HTS-1 is 0.55 nm. Reactant molecular cyclohexane can easily enter the intra-crystalline voids of the W/HTS material via the micropore. The bulky cyclohexanol intermediate formed within the intracrys-

talline voids, however, will be held in the vicinity of the active sites until the reaction proceeds further to yield the more mobile cyclohexanone and/or desired linear product AA. As already shown in Table 1 (entry 2), the better of the selectivity to cyclohexanone was obtained on the pure HTS-1 material, which is proved directly for the role of hollow structure. Additionally, the 50% W/HTS material was calcined at 150, 300, 500, 650 °C respectively and the corresponding activities were also investigated under the same conditions. As shown in Fig. 8A, the best activity and selectivity to AA were observed on the catalysts calcined 500 °C, but dropped for the catalysts calcined above or below 500 °C. Based on the XRD and Raman spectroscopy (Fig. 1B and Fig. 5B), no significant isolated small $(\text{WO}_3)_n$ clusters species crystallization was shown at calcination temperatures of 300 °C and lower, while the isolated small $(\text{WO}_3)_n$ clusters species re-structured and gradually crystallized with increasing calcination temperature from 300 to 650 °C. This fact suggested that the tungsten species might not be fully activated to form some intermediate valence state and polytungstate structure at lower calcination temperature, additionally the interaction at the tungsten species and HTS-1 interface was not sufficiently strong to inhibit leaching of the active tungsten species during the reaction. The formation of the crystalline WO_3 domains, however, led to decrease activity at higher calcination temperature. Based on characterization results by N_2 physisorption (Table S1), this fact suggested that the low catalytic activity for the catalyst calcinated at higher temperature (650 °C) might be attributed to the decrease of BET-specific surface area and pore size.

In order to further understand the product distribution in the cyclohexane oxidation, we studied the effect of reaction parameters. The effect of the temperature on the cyclohexane conversion and product selectivities is investigated and plotted in Fig. 9A. The conversion of cyclohexane and AA selectivity gradually increased with increasing temperature and reached a maximum at 90 °C, whereas the selectivities to KA oil intermediates rapidly decreased. It was clear that cyclohexane was first converted into KA oil intermediates and then further converted into AA. This indicated that reaction energy was not enough for the oxidative cleavage of KA oil at low temperature, and AA was hardly to be formed. Further increasing the temperature to 120 °C resulted in a rapid decrease in the conversion and the AA selectivity to 12 and 41%, respectively. The decrease in the cyclohexane conversion at high temperature may be attributed to easier self-decomposition of H_2O_2 reactant. More important, degradation rate of AA rapidly increased at higher temperature. Fig. 9B shows the effect of reaction time on both cyclohexane conversion and AA selectivity. It is well observed that with increasing time, initially the cyclohexane conversion (till 14 h) increases rapidly, but after 14 h the cyclohexane conversion increases slightly. Meanwhile, the selectivity of AA first increased and then decreased and the selectivity of KA oil intermediates was gradually decreased with the reaction time. Further increasing the reaction time causes the decline of AA yield, implying occurrence of AA degradation by deep oxidation at the too much elongated reaction time. We have also explored the effect of the catalyst amount on catalytic behaviour. As shown in Fig. 9C, there was an almost proportional effect of the catalyst amount on cyclohexane conversion and AA selectivity (with a catalyst amount as low as 0.1 g). Afterwards, a rapid decrease in the AA selectivity happens at the higher catalyst amount over 0.1 g, due to the over-oxidation on the too much number of catalytically active sites. Additionally, the decomposition rate of H_2O_2 increased with increasing catalyst amount. The influences of H_2O_2 /cyclohexane molar ratio on the cyclohexane oxidation were following evaluated and the results are shown in Fig. 9D. A similar curve with Fig. 9A was observed, where the cyclohexane conversion and AA selectivity increased simultaneously and the selectivity of KA oil intermediates gradually decreased with increasing H_2O_2 /cyclohexane molar ratio. Due

to unproductive decomposition of H_2O_2 , oxidation of cyclohexane to AA required more H_2O_2 than cyclohexane to proceed to a high level. The optimum H_2O_2 /cyclohexane molar ratio was proved to be 3:1; further increment of H_2O_2 amount resulted in a significant decrease in cyclohexane conversion, probably due to the fact that, self-decomposition of H_2O_2 produced excess water in the reaction mixture and thereby contact of cyclohexane (immiscible in water), catalyst and H_2O_2 (highly soluble in water) was interrupted. Furthermore, the existence of too much free H_2O_2 in the reaction system accelerated the decomposition of AA to other products by over-oxidation.

From the context of a 'green' approach, the oxidative conversion of cyclohexane to AA was carried out with a reused W/HTS catalyst under the same experimental conditions. After each catalytic cycle, the used catalyst is recovered facily from the reaction mixture by centrifugation, washed thoroughly with ethanol for three times, and kept for drying at 120 °C overnight prior to the next cycle. As shown in Fig. 8B, the catalyst after 4 consecutive experiments did not lead to any significant decline in its efficiency in terms of conversion and selectivity and was proved to be truly of a heterogeneous nature. A similar phenomenon was also reported by Dai et al. [44] when using tungsten-based SBA-15 catalyst in the selective oxidation of cyclopentene with H_2O_2 , demonstrating the presence of strong interactions between active tungsten species and the silica-based matrix. Meanwhile, after completion of the reaction, the solid catalyst was removed from the reaction mixture by filtration during the hot conditions and the resulting filtrate was independently analyzed by ICP-AES analysis. It was found that Ti or W ions were hardly detected in the filtrate, which supported the fact that the catalyst is devoid of leaching properties; this can be due to the fact that Ti and W ions remain strongly anchored upon the silica-based matrix.

3.3. Active sites related to the reaction mechanism

The excellent catalytic activity of W/HTS for direct conversion of cyclohexane to adipic acid can be explained by the combination of bifunctional catalytic sites and hollow sphere-like structure as well as surface strong acidic properties. First, HTS is composed of the Ti-O_x species existing in a tetrahedral coordination (Ti-O_4 species), which are generally regarded as catalytic active centers for activation of the C–H bonds of cyclohexane [27]. This result has also been testified in a separate experiment with the addition of pure HTS-1 instead of W/HTS, the formation of KA oil intermediates as major products (96%) at reaction conditions was proved directly (Table 1). Additionally, a 82.3% cyclohexanone yield was produced on this HTS-1 catalyst for oxidation of cyclohexanol under the same conditions. As stated above, it can be deduced that the formation of cyclohexanol should occur over Ti-O_4 species from cyclohexane, and the further conversion of cyclohexanol to cyclohexanone should also occur over Ti-O_4 species. Meanwhile, this hollow-structured HTS-1 tends to favor the formation of cyclohexanone for the aforementioned target reactions, as compared to traditional solid TS-1 [28]. This can be explained with re-distribution of Ti species during dissolution-recrystallization process in the following way: the Ti and Si species are gradually dissolved with the presence of TPAOH, the dissolved Ti species can be regrown onto the surface of HTS crystals and the Ti species on the surface are more accessible than those in the core of the solid-structured TS-1 crystals [33]. On the other hand, it is probably due to its intra-particle voids of HTS, which can enhance the accessibility of active centers and diffusion of product molecules throughout the shell of the catalysts.

From the above detailed investigation of the catalytic performance of the W/HTS catalysts, tungsten species seem to play vital roles in the C–C cleavage of cyclohexanone to AA. To further verify

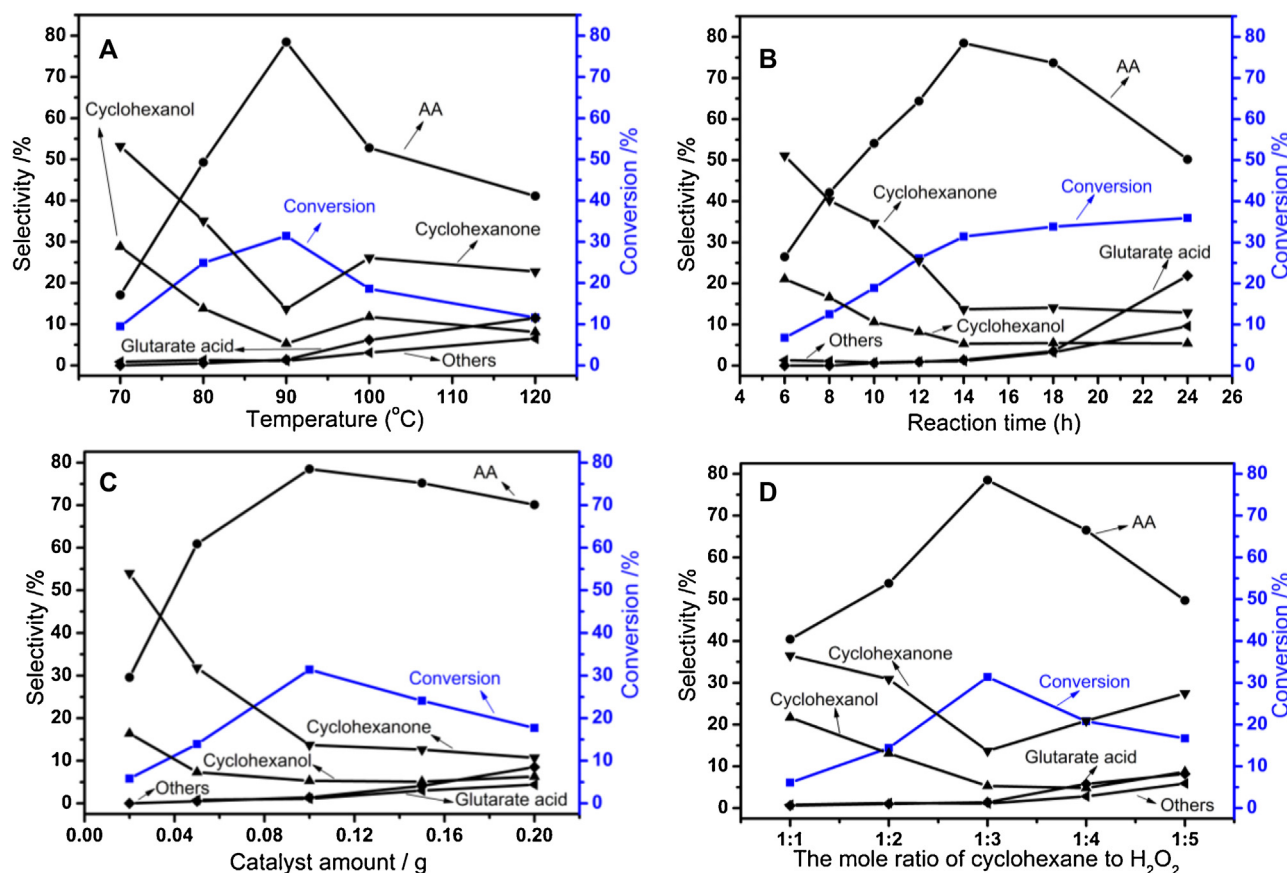


Fig. 9. Effect of the temperature (A), reaction time (B), catalyst amount (C) and mole ratio of cyclohexane to H₂O₂ (D) on the conversion of cyclohexane and AA, cyclohexanol, cyclohexanone and glutarate acid selectivity over the synthesized 50% W/HTS catalysts.

the roles of tungsten species, reactivity of KA oil intermediates over H₂WO₄-modified Silicate-1 was investigated. Cyclohexanol and cyclohexanone were oxidized to AA in a higher reaction rate than cyclohexane, respectively. Further, the reactivity of cyclohexanone was compared with that of cyclohexanol over H₂WO₄-modified catalyst systems and cyclohexanone showed a higher AA yield in the oxidation reaction (Tables 1, entries 13 and 14). This work also has investigated nature and structure of the tungsten species in detail. UV–vis DRS results demonstrate that at low H₂WO₄ content (< 25 wt%), the H₂WO₄-modified HTS-1 consists mainly of highly dispersed tungsten species and low-condensed oligomeric tungsten species entities. At higher H₂WO₄ loading, the conglomeration degree of tungsten species increases, and bulk WO₃ species appear. FT-IR characterizations of the W/HTS catalysts have confirmed that there is a strong interaction between the tungsten species and the support, preventing leaching of the tungsten species during the selective oxidation reaction. Investigation by means of XPS indicates that two types of tungsten species with oxidation states of +6 and +5 exist in the W/HTS catalyst. Additionally, increasing calcination temperature from 150 to 650 °C led to structural evolution of supported tungsten active species and subsequent activity change. The structure of H₂WO₄ can be dissociated around 300 °C causing the formation of various WO_x species. These WO_x species may bond to Si atoms on HTS-1 surface through W–O–Si interaction and possess some intermediate valence state and polytungstate structure. Condensation of isolated tungsten species between neighboring WO_x groups increased with calcination temperature and an amount of bulk WO₃ were formed above 500 °C. However, the selectivity of KA oil intermediates dropped while that of AA could reach its maximum value with increase of the

catalyst calcination temperature to 500 °C, which indicates the terminal W=O group in the bulk WO₃ is also the active site. As a result, the nature and structure of the tungsten species strongly depend on H₂WO₄ loading and calcination temperature, as shown in Fig. 10. The isolated tungsten species with four kinds of structures are predominant in catalysts with low H₂WO₄ loading and calcination temperature, which is the active site for the conversion of KA oil intermediate. Increasing the H₂WO₄ loading and calcination temperature lead to the formation of low condensed oligomers of tungsten species with the catalytic activity. Finally, with further increasing polymerization degree of the tungsten species, the bulk WO₃ appears. These mixed tungsten species possessing some intermediate valence state and polytungstate structure show a higher catalytic activity in selective oxidation of KA oil intermediates to AA.

Under normal conditions, hydrogen peroxide does not interact with cyclohexane. Ti–O₄ and tungsten species, however, are expected to react with hydrogen peroxide to form peroxo complexes, which are able to abstract hydrogen atoms from cyclohexane. Further dissociation of peroxo complexes formed over the catalyst generates active •OH free radicals that are stabilized by the solvent acetone to a great extent. Considering the experimental results from the W/HTS catalysts above, oxidation of cyclohexane by a •OH free radicals seems to occur over the Ti-based peroxo complex at any of the 12 equivalent C–H bonds. In the case of later intermediates such as cyclohexanol and cyclohexanone, oxidative functionalization of C–H bond can only occur over the W-based peroxo complex exclusively at the weakest α–C–H bond adjacent to the electron-withdrawing hydroxyl or carbonyl group. Note that methylene C–H (~99 kcal/mol) bond strengths for cyclohexane are,

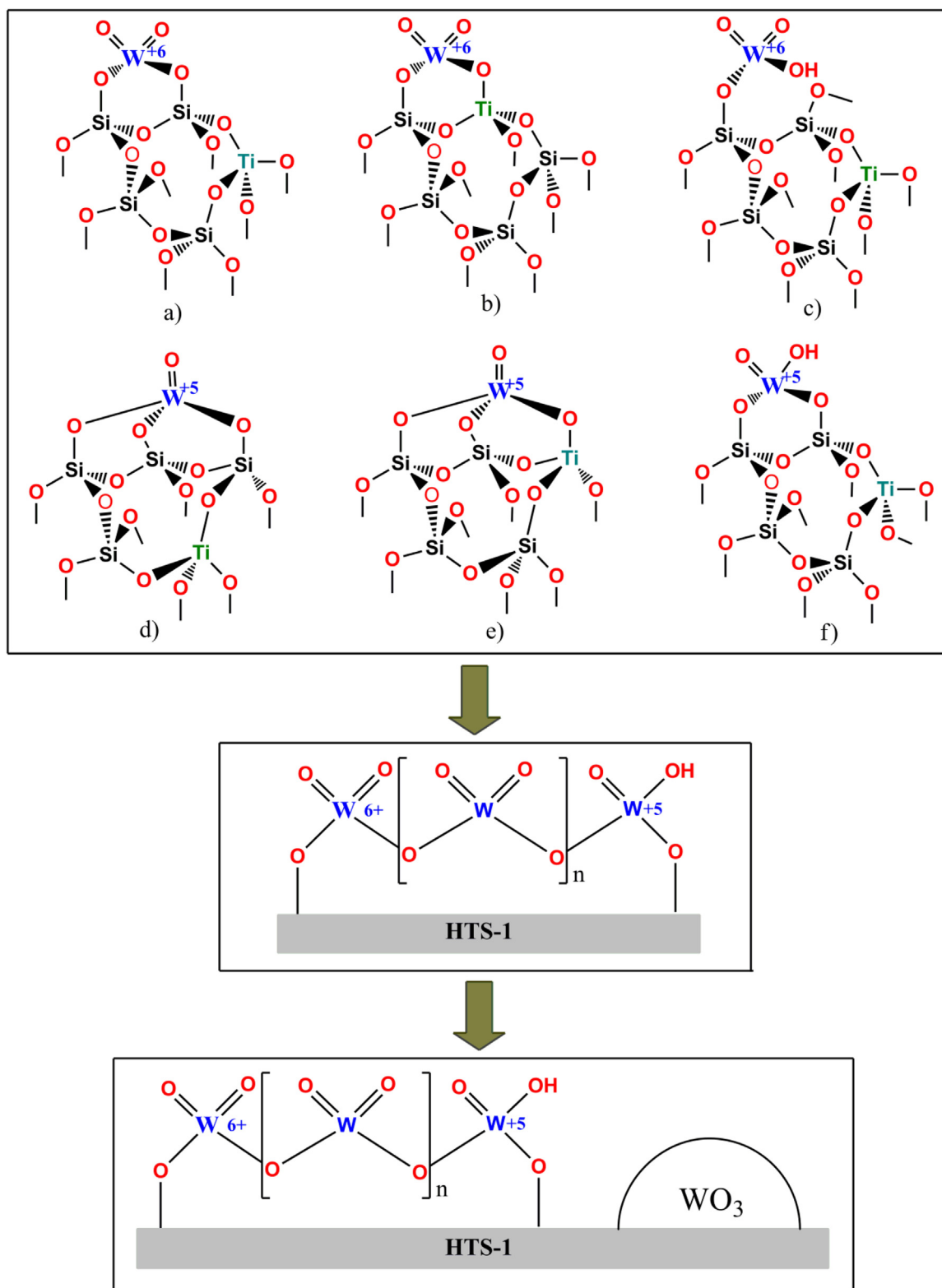


Fig. 10. Scheme of structure (proposed model) evolution of supported tungsten species with different calcination temperature and H_2WO_4 loading.

in general, stronger than that of $\alpha\text{-C-H}$ bonds (~ 97 kcal/mol) for cyclohexanol and cyclohexanone. Thus we are very interested in the roles of two types of peroxo complexes, and we want to further compare the catalytic activities between tungsten peroxo complex and Ti peroxo complex for oxidative functionalization of C–H bonds. Based on the reports [30,31], the two possible types of active

structures for W and Ti peroxo complexes have been suggested, which include peroxo active structure, as shown in Fig. 11A and 11B. This is a highly simplified system, and DFT calculations were carried out to only elucidate the electronic distribution and band distance of the different peroxo active structures. Fig. 11C and 11D show the optimized structures of TiO_6H_6 (a) and WO_6H_3 (b) models includ-

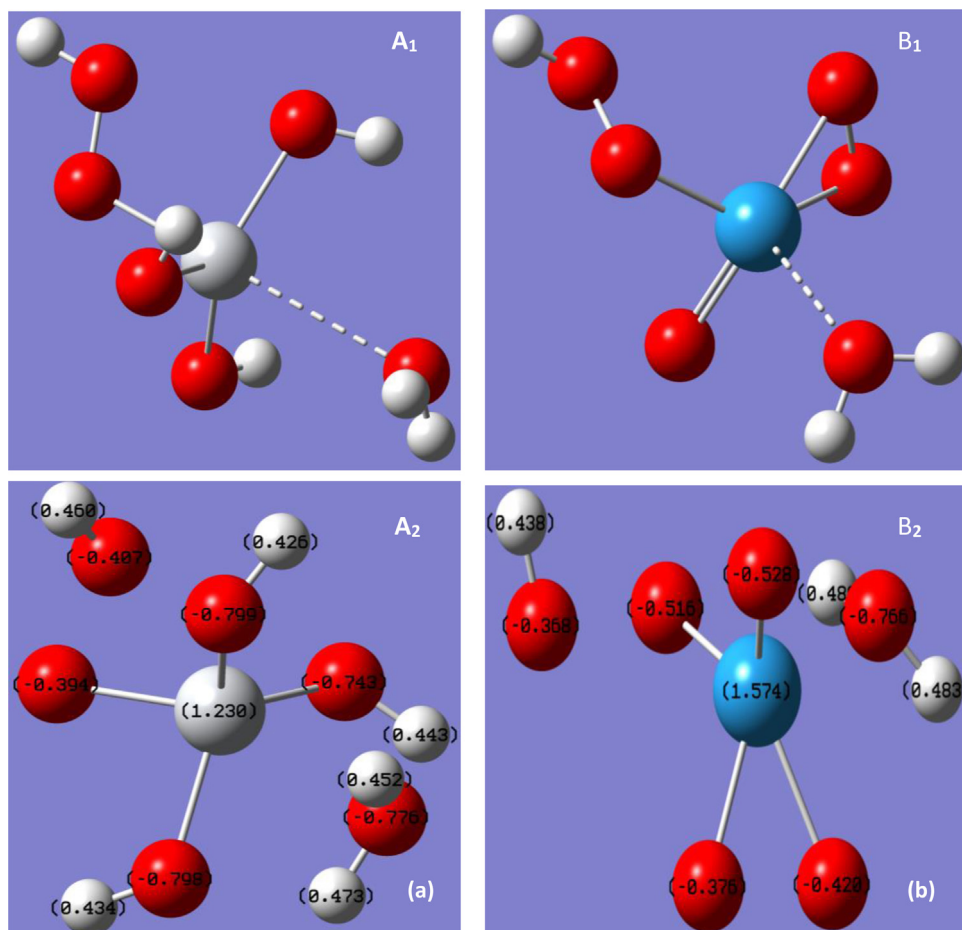


Fig. 11. Suggested simple models and electronic structure of optimized models for the different active (a) and (b).

ing the calculated atomic Milikan charge of selective Ti, W and O(1) atoms in the O(2)–O(1)–H group taken from the peroxo active sites, respectively. In the (a) model, the Ti–O(2) bond length (1.884 Å) in the Ti–O(2)–O(1)–H group is approximately 1 ~ 9% longer than the other framework Ti–O bond length. The other framework Ti–O bond lengths in the optimized TiO₆H₆ are 1.810 ~ 1.862 Å, which agrees well with EXAFS measurements of Ti–O bond lengths in the tetrahedral coordination (1.81 ± 0.02 Å) [61]. In the (b) model, the distance of the W–O(2) bond is 1.945 Å, whereas other W–O distances are 1.914 and 1.944 Å respectively in the annular tungsten sites; the W=O bond lengths 1.708 Å. These data are also in accordance with those reported in previous work [31]. The distance between the metal center and the ligand donor O atom (H₂O) ranges between 2.22 and 2.47 Å for both models, are very similar to literature data [62]. Of interest is that in both peroxo complexes O(1)–O(2) bond distances (1.462 Å for Ti peroxo bond and 1.463 Å for W peroxo bond, respectively) are larger than that in H₂O₂ (1.32 Å), which is easy for homolytic cleavage of the longer O–O bond to produce •OH free radicals and follows the mechanism proposed by Kazarnovsky [63]. Additionally, the different charges of O(1) atoms located at the peroxo sites in the different models are observed; the charge (0.407 e) of adjacent O (1) atom in Ti–O(2)–O(1)–H sites is higher than that (0.368 e) of in W–O(2)–O(1)–H sites due to the obvious change of p state electron by Ti atom. Thus, the formed Ti peroxo sites behave as a stronger nucleophile and proceed towards the H-atom bearing a partial positive charge. Consequently, a homolytic cleavage of the C–H bond of cyclohexane occurs easily over the Ti peroxo sites to form cyclohexyl radicals and thus benefiting the catalytic performance. Besides, In the (b) model with W–O(2)–O(1)–H

sites, the Milikan charge (1.574 e) of W atom is higher than that (1.230 e) of Ti atom in Ti–O(2)–O(1)–H sites, showing that the electrophilic feature of W peroxo complex is much stronger than that Ti peroxo complex. As a result, W site is the relatively better coordination of later KA oil intermediates with electronegative groups than cyclohexane, resulting in a lower reaction energy barrier. This might facilitate a rupture of a C_{sp}²–C_{sp}² bond of later intermediates under heating in realizing catalysis cycle.

The W surface sites owing to the strong interaction with the HTS-1 surface can result in them strong proton release ability and thereby high acid strength [64]. Strong acid sites tend to favor the tautomerism of cyclohexanone to the corresponding enolic form, which is more easily activated by radical H abstraction than cyclohexanone itself to produce radical species for the aforementioned target reactions [29]. According to the NH₃-TPD results, the formation of strong acid sites over the H₂WO₄ modified HTS-1 catalysts have been further confirmed. The role of surface acidic sites has also been testified in a separate experiment with the addition of Na₂WO₄-modified HTS-1 instead of H₂WO₄-modified HTS-1, the formation of AA with a low selectivity (18%) at reaction conditions was proved directly (Table 1). Additionally, hollow structure of W/HTS leads to them excellent mesoporosity with well-distributed pores, which can provide better dispersion of the tungsten species onto the surface of intra-particle voids throughout the shell of the catalysts and enhance the population of surface strong acidic sites. The accessibility of the KA oil intermediates to surface strong acidic sites, therefore, can be increased, having a positive influence on oxidation cleavage of KA oil intermediates to AA.

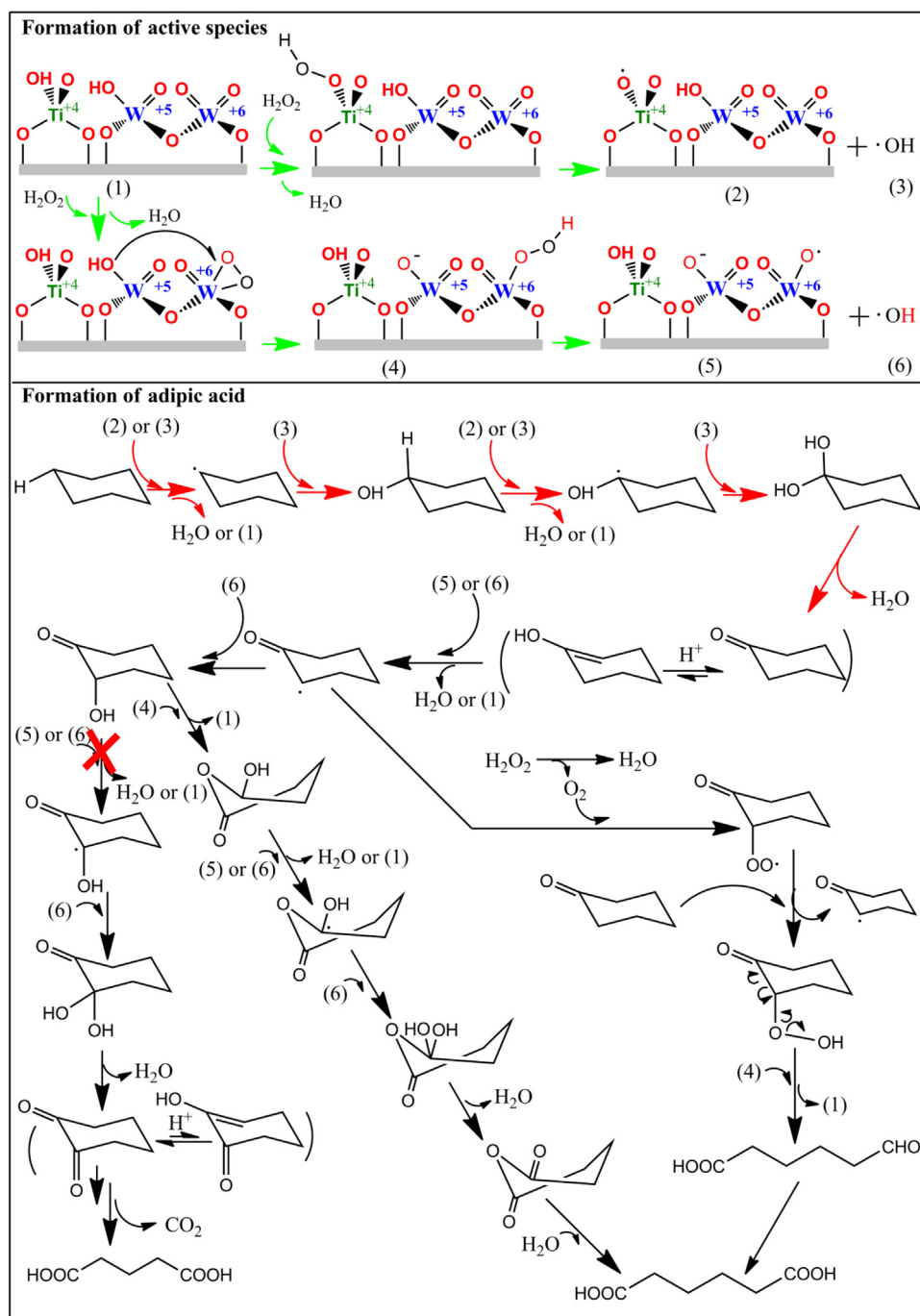


Fig. 12. Mechanistic pathway for oxidative conversion of cyclohexane to AA.

3.4. Reaction mechanism

Currently, the widely accepted mechanism for the oxidation of cyclohexane proceeds by a free radical process [63,65]. To verify the possibility that this reaction is radical based using the W/HTS as catalysts, a free radical scavenger (hydroquinone) was added to the cyclohexane oxidation system (Table 1, entry 16). It was found that the radical scavenger had a strong inhibitory effect on the cyclohexane reaction and therefore occurs by a free-radical mechanism. To assess whether subsequent stages of the overall reaction of cyclohexane also proceed participation of free radicals, the later intermediate cyclohexanone as the starting reagent in the presence of hydroquinone scavenger were carried out (Table 1, entry 17).

The results were the same in the case and the radical scavenger evidently suppresses all production of the AA, showing that the conversion of later cyclohexanone intermediate to AA also involves the traditional radical mechanism.

Fig. 12 shows possible mechanism of one-single catalytic oxidation of cyclohexane to AA over the W/HTS. The mechanism was proposed based on the above computational and experimental studies carried out in the presence and absence of various types of heterogeneous catalysts with cyclohexane and some stable intermediates (cyclohexanone and cyclohexanol) as reactants. In the first step of reaction, the active Ti–O₄ species on the catalyst reaction with hydrogen peroxide to form Ti peroxo complexes with a higher electronegative adjacent O (1) atom, facilitating posi-

tive hydrogen attraction from the C–H bond of cyclohexane. At the same time, Ti peroxo complexes dissociate to generate Ti-centered radical species ($\text{Ti}^{4+}\text{--O}\cdot$) and a hydroxyl radical ($\cdot\text{OH}$) [66]. These obtained radicals are highly reactive and can abstract one absorbed H from cyclohexane to form cyclohexyl radicals, followed by addition of another $\cdot\text{OH}$ to form a cyclohexanol [28]. The formed cyclohexanol is further oxidized with the production of $\cdot\text{OH}$ at the weakest methine C–H bond (~ 96 kcal/mol) to form a geminal diol, 1,1'-dihydroxycyclohexane. Geminal diol is well-known to be very unstable and will rapidly undergo dehydration to product stable cyclohexanone [67]. The formation of a C–O bond in cyclohexane requires cleavage of one C–H bond, which is exothermic and thermodynamically favored; subsequent formation of a C=O bond with cleavage of a methine C–H bond in cyclohexanol is also thermodynamically favored. Note that methylene C–H (~ 99 kcal/mol) bond strength of cyclohexane is, in general, stronger than that of α -C–H bonds cyclohexanol (~ 97 kcal/mol). Selective formation of cyclohexanol in this stage is a key step in the direct conversion of cyclohexane to adipic acid and its yield directly affects the yield of AA. This is in agreement with the observed catalytic results obtained using pure HTS-1 catalysts, having a higher cyclohexanone selectivity. Therefore the catalytic centers for cyclohexane conversion to cyclohexanol are mainly tetrahedral Ti species. Ti species can also cause consecutive oxidation of cyclohexanol to cyclohexanone, acting as active sites for cleavage of the C–H bond of adsorbed cyclohexanol. However, these centers are catalytically less active for cyclohexanone reaction proceeding in the second step.

In the second step, the tungsten species are the active sites in oxidation of later KA oil intermediates to AA in present bifunctional catalysts. This is similar to Sato et al.'s results that H_2WO_4 shows high reactivity for cyclohexanol or cyclohexanone oxidation to AA [23]. This can also be confirmed by the following facts: (i) high reactivity of possible KA oil intermediates over H_2WO_4 -modified Silicate-1, whereas low catalytic activity for cyclohexane oxidation was obtained under similar conditions; (ii) the formation of AA strongly depends on tungsten species content during the cyclohexane oxidation; (iii) the changes in activity are consistent with the observed structural evolution of tungsten species on these supports by calcination temperature and H_2WO_4 loading. Based on the computational results, the tungsten species react with H_2O_2 to generate W peroxo complexes with a higher positive W atom (compared to Ti atom in Ti peroxo complexes), facilitating coordination of later intermediates with electronegative groups (i. e., cyclohexanol, cyclohexanone). The H-abstraction at the weakest C–H bond adjacent to the carbonyl position in cyclohexanone (or adjacent to a double bond in enol-form isomers by tautomerism) by formed $\cdot\text{OH}$ can most likely be promoted in the presence of W species coordination [68], and the production of radical at this position readily leads to the formation of 2-hydroxycyclohexanone and α -keto hydroperoxide. 2-hydroxycyclohexanone may undergo a pathway to generate hydroxy-lactone, which then reacts with H_2O_2 to form acid anhydride, followed by hydrolysis, and to produce AA [69]. Separate experiments confirm that hydroxy-lactone can be converted to AA under the same condition, whereas cyclohexanediketone was converted to pentanedioic acid instead of AA. Additionally, α -keto hydroperoxide may decompose to generate carboxylic acid-aldehyde, and then to adipic acid by H_2O_2 oxidation of the aldehyde moiety as shown in Fig. 12. The above reaction mechanism for $\cdot\text{OH}$ radical-mediated oxidative conversion of cyclohexane to cyclohexanol, followed by oxidation of cyclohexanol and finally to adipic acid was supported by reaction intermediates detection during the reaction time course.

4. Conclusion

To summarize, we have shown a simple and non- HNO_3 route for the highly selective direct synthesis of adipic acid by oxidation of cyclohexane with 30% H_2O_2 over hollow $\text{H}_2\text{WO}_4/\text{TS-1}$ bifunctional catalysts in this work. It has been demonstrated that bifunctional $\text{H}_2\text{WO}_4/\text{TS-1}$ with intracrystalline voids was efficient catalyst for the direct transformation of cyclohexane to adipic acid with 30% H_2O_2 . High activity originates from the combination of unique hollow spherical morphology of catalyst, synergistic effects between Ti--O_4 species and surface W species and strong acid sites. Unique hollow spherical morphology could shorten the diffusion distance and facilitate mass transport of the reactants and products. The virtue of such synergic effect was reflected in reaction steps: tetrahedral Ti species catalyze cyclohexane oxidation to KA oil intermediate and tungsten sites catalyze KA oil further oxidation to adipic acid. Strong acid sites tend to favor the tautomerism of cyclohexanone to the corresponding enolic form, which is easily activated by radical H abstraction than cyclohexanone itself to produce radical species for the aforementioned target reactions. The changes in activity for AA formation are consistent with the observed structural evolution of tungsten species on HTS-1 supports by calcination temperature and tungsten species content. In this contribution, an innovative approach to direct produce AA from cyclohexane avoids the nitric oxidation route which generates a strong greenhouse gas, and thus provides an environmentally benign alternative for an important industrial reaction.

Acknowledgments

This work was supported by the Natural Science Foundation of China (Grant No.21576078) and Scientific Research Fund of Hunan Provincial Education Department (Grant No.15C0816) and the Natural Science Foundation of Hunan Province (Grant No.14JJ2056).

Appendix A. Supplementary data

Supplementary data associated with this article can be found, in the online version, at <http://dx.doi.org/10.1016/j.apcatb.2016.04.005>.

References

- [1] A. Corma, S. Iborra, A. Velty, *Chem. Rev.* 107 (2007) 2411–2502.
- [2] S. Ghosh, S.S. Acharyya, S. Adak, L.N. Sivakumar Konathala, T.S.R. Bal, *Green Chem.* 16 (2014) 2826–2834.
- [3] S.S. Acharyya, S. Ghosh, R. Bal, *Green Chem.* 17 (2015) 3490–3499.
- [4] K.C. Hwang, A. Sagadevan, *Science* 346 (2014) 1495–1498.
- [5] U. Schuchardt, D. Cardoso, R. Sercheli, R. Pereira, R.S. Cruz, M.C. Guerreiro, D. Mandelli, E.V. Spinace, E.L. Pires, *Appl. Catal. A: Gen.* 211 (2001) 1–17.
- [6] Y. Wu, C. Cordier, E. Berrier, N. Nuns, C. Dujardin, P. Granger, *Appl. Catal. B: Environ.* 140–141 (2013) 151–163.
- [7] D. Pietrogioacomi, M.C. Campa, L.R. Carbone, S. Tuti, M. Occhiuzzi, *Appl. Catal. B: Environ.* 187 (2016) 218–227.
- [8] M. Piumetti, M. Hussain, D. Fino, N. Russo, *Appl. Catal. B: Environ.* 165 (2015) 158–168.
- [9] G. Grzybnek, P. Stelmachowski, S. Gudyka, P. Indyka, Z. Sojka, N. Guillén-Hurtado, V. Rico-Pérez, A. Bueno-López, A. Kotarb, *Appl. Catal. B: Environ.* 180 (2016) 622–629.
- [10] T. Iwahama, K. Syojo, S. Sakaguchi, Y. Ishii, *Org. Process Res. Dev.* 2 (1998) 255–260.
- [11] S.A. Chavan, D. Srinivas, P. Ratnasamy, *J. Catal.* 212 (2002) 39–45.
- [12] H. Lü, W. Ren, P. Liu, S. Qi, W. Wang, Y. Feng, F. Sun, Y. Wang, *Appl. Catal. A: Gen.* 136 (2012) 441–442.
- [13] M. Dugal, G. Sankar, R. Raja, J.M. Thomas, *Angew. Chem. Int. Ed.* 112 (2000) 2399–2402.
- [14] G. Zou, W. Zhong, Q. Xu, J. Xiao, C. Liu, Y. Li, L. Mao, S. Kirk, D. Yin, *Catal. Commun.* 58 (2015) 46–52.
- [15] H. Li, Y. She, H. Fu, M. Cao, J. Wang, T. Wang, *Can. J. Chem.* 93 (7) (2015) 696–701.

- [16] X. Shenga, N. Daemsa, B. Geboes, M. Kurttepel, S. Bals, T. Breugelmans, A. Hubin, I.F.J. Vankelecom, P.P. Pescarmon, *Appl. Catal. B: Environ.* 176–177 (2015) 212–224.
- [17] W.T. Hess, in: J.I. Kroschwitz, M. Howe-Grant (Eds.), *Kirk-Othmer Encyclopedia of Chemical Technology*, vol. 13, 4th ed., John Wiley & Sons, Inc., New York, 1995, pp. 961–995.
- [18] R. Saliger, N. Decker, U. Prüße, *Appl. Catal. B: Environ.* 102 (2011) 584–589.
- [19] K. Sato, M. Aoki, R. Noyori, *Science* 281 (1998) 1646–1647.
- [20] W. Zhu, H. Li, X. He, *Catal. Commun.* 9 (2008) 551–555.
- [21] M. Vafaezadeh, M.M. Hashemi, *Catal. Commun.* 43 (2014) 169–172.
- [22] M. Shang, T. Noël, Q. Wang, Y. Su, K. Miyabayashi, V. Hessel, J. Chem. Eng. (2015) 454–462.
- [23] Y. Usui, K. Sato, *Green Chem.* 5 (2003) 373–375.
- [24] K. Nomiya, M. Miwa, Y. Sugaya, *Polyhedron* 3 (1984) 607–610.
- [25] R.A. Sheldon, J. Dakka, *Catal. Today* 19 (1994) 215–245.
- [26] X. Ye, Y. Cui, X. Qiu, X. Wan, *Appl. Catal. B: Environ.* 152–153 (2014) 383–389.
- [27] E.V. Spinace, H.O. Pastore, U. Schuchardt, *J. Catal.* 157 (1995) 631–635.
- [28] C. Shi, B. Zhu, M. Lin, J. Long, R. Wang, *Catal. Today* 175 (2011) 398–403.
- [29] G. Zou, W. Zhong, L. Mao, Q. Xu, J. Xiao, D. Yin, Z. Xiao, S.R. Kirk, T. Shu, *Green Chem.* 17 (2015) 1884–1892.
- [30] W. Panyaburapa, T. Nanok, J. Limtrakul, *J. Phys. Chem. C* 111 (2007) 3433–3441.
- [31] L. Barrio, J.M. Campos-Martín, J.L.G. Fierro, *J. Phys. Chem. A* 111 (2007) 2166–2171.
- [32] J. Wang, L. Xu, K. Zhang, H. Peng, H. Wu, J. Jiang, Y. Liu, P. Wu, *J. Catal.* 288 (2012) 16–23.
- [33] Y. Wang, M. Lin, A. Tuel, *Micropor. Mesopor. Mater.* 102 (2007) 80–85.
- [34] W. Zhong, T. Qiao, J. Dai, L. Mao, Q. Xu, G. Zou, X. Liu, D. Yin, F. Zhao, *J. Catal.* 330 (2015) 208–221.
- [35] J.R. Agger, N. Hanif, M.W. Anderson, *Angew. Chem. Int. Ed.* 40 (2001) 4065–4067.
- [36] C.-Y. Su, H.-C. Lin, *J. Phys. Chem. C* 113 (2009) 4042–4046.
- [37] A.B. Kulal, M.K. Dongare, S.B. Umbarkar, *Appl. Catal. B: Environ.* 182 (2016) 142–152.
- [38] M.S. Morey, J.D. Bryan, S. Schwarz, G.D. Stucky, *Chem. Mater.* 12 (2000) 3435–3444.
- [39] S.-Y. Chen, T. Mochizuki, Y. Abe, M. Toba, Y. Yoshimura, P. Somwongsab, S. Lao-ubol, *Appl. Catal. B: Environ.* 181 (2016) 800–809.
- [40] M. Shihata, Z. Gabelica, *Zeolites* 19 (1997) 246–252.
- [41] N.V. Maksimchuka, I.D. Ivanchikova, A.B. Ayupov, O.A. Kholdeev, *Appl. Catal. B: Environ.* 181 (2016) 363–370.
- [42] H. Zhang, Y. Liu, Z. Jiao, M. He, P. Wu, *Ind. Eng. Chem. Res.* 48 (2009) 4334–4339.
- [43] E. Iglesia, D.G. Barton, S.L. Soled, S. Miseo, J.E. Baumgartner, W.E. Gates, G.A. Fuentes, G.D. Meitzner, *Stud. Surf. Sci. Catal.* 101 (1996) 533–542.
- [44] X. Yang, W. Dai, R. Gao, K. Fan, *J. Catal.* 249 (2007) 278–288.
- [45] G.N. Vayssilov, *Catal. Rev.-Sci. Eng.* 39 (1997) 209–244.
- [46] G. Tozzola, M.A. Mantegazza, G. Ranghino, G. Petrini, S. Bordiga, G. Ricchiardi, C. Lamberti, A. Zulian, *J. Catal.* 179 (1998) 64–71.
- [47] B. Part, S.Y. Hou, Z.H. Zhou, T.R. Lin, H.L. Wan, *Eur. J. Inorg. Chem.* 2006 (2006) 1670–1677.
- [48] B. Ingham, S.V. Chong, J.L. Tallon, *J. Phys. Chem. B* 109 (2005) 4936–4940.
- [49] B. Hu, H. Liu, K. Tao, C. Xiong, S. Zhou, *J. Phys. Chem. C* 117 (2013) 26385–26395.
- [50] D.G. Barton, M. Shtein, R.D. Wilson, S.L. Soled, E. Iglesia, *J. Phys. Chem. B* 103 (1999) 630–640.
- [51] C. Li, G. Xiong, J. Liu, P. Ying, Q. Xin, Z. Feng, *J. Phys. Chem. B* 105 (2001) 2993–2997.
- [52] D.M. David Jeba Singh, T. Pradeep, K. Thirumoorthy, K. Balasubramanian, *J. Phys. Chem. A* 114 (2010) 5445–5452.
- [53] K. Assaker, C. Carteret, M.-J. Stébé, J.-L. Blin, *Micropor. Mesopor. Mater.* 194 (2014) 208–218.
- [54] H. Atia, U. Armbruster, A. Martin, *J. Catal.* 258 (2008) 71–82.
- [55] Y. Hasegawa, A. Ayame, *Catal. Today* 71 (2001) 177–187.
- [56] S. Doniach, M. Sunjic, *J. Phys. C: Solid State Phys.* 3 (1970) 285–291.
- [57] R.J. Colton, J.W. Rabalais, *Inorg. Chem.* 15 (1976) 236–238.
- [58] M.A. Corteis-Jaícome, C. Angeles-Chavez, E. Loípez-Salinas, J. Navarrete, P. Toribio, J.A. Toledo, *Appl. Catal. A: Gen.* 318 (2007) 178–189.
- [59] X.L. Yang, R.H. Gao, W.L. Dai, K.N. Fan, *J. Phys. Chem. C* 112 (2008) 3819–3826.
- [60] Y. Baek, K. Yong, *J. Phys. Chem. C* 111 (2007) 1213–1218.
- [61] T. Blasco, A. Corma, M.T. Navarro, J.P. Pariente, *J. Catal.* 156 (1995) 65–74.
- [62] R.R. Sever, T.W. Root, *J. Phys. Chem. B* 107 (2003) 4080–4089.
- [63] I.A. Kazarnovsky, *Dokl. AN SSSR* 221 (1975) S353 (in Russian).
- [64] F. Figueras, J. Palomeque, S. Loricant, C. Fèche, N. Essayem, G. Gelbard, *J. Catal.* 226 (2004) 25–31.
- [65] L. Gómez-Hortigüela, F. Corà, G. Sankar, C.M. Zicovich-Wilson, C.R.A. Catlow, *Chem. Eur. J.* 16 (2010) 13638–13645.
- [66] W. Zhou, R. Wischert, K. Xue, Y. Zheng, B. Albela, L. Bonneviot, J.-M. Clacens, F.D. Campo, M. Pera-Titus, P. Wu, *ACS Catal.* 4 (2014) 53–62.
- [67] I. Ignatyev, M. Montejó, P.G.R. Ortega, J.J.L. González, *Phys. Chem. Chem. Phys.* 13 (2011) 18507–18515.
- [68] S. Mitroka, S. Zimmeck, D. Troya, J.M. Tanco, *J. Am. Chem. Soc.* 132 (2010) 2907–2913.
- [69] S.-O. Lee, R. Raja, K.D.M. Harris, J.M. Thomas, B.F.G. Johnson, G. Sankar, *Angew. Chem.* 115 (2003) 1558–1561.